The lateral septum plays a transforming role in acute stress-induced analgesia

Devanshi Shah[#], Pallavi Sharma*, Rachit Agarwal*, and Arnab Barik[#]

[#]Centre for Neuroscience, Indian Institute of Science, Bengaluru, Karnataka, India - 560012
*Centre for BioSystems Science and Engineering, Indian Institute of Science, Bengaluru, Karnataka, India - 560012

Corresponding author: arnabbarik@iisc.ac.in

Abstract

Stress is a powerful modulator of pain. Specifically, acute stress due to physical restraint facilitates stress-induced analgesia (SIA). However, where, and how acute stress and pain pathways interface in the brain must be better understood. Here, we describe how the lateral septum (LS), a forebrain limbic nucleus, facilitates SIA through its downstream targets in the lateral hypothalamus (LH). We show that the LS→LH circuitry is sufficient to drive analgesia and is required for SIA. Further, we reveal that the LS→LH pathway is opioid-dependent and modulates pain through the pro-nociceptive neurons in the rostral ventromedial medulla (RVM). Remarkably, we found that the LS neurons are inhibitory, are recruited specifically when the mice struggle to escape under restraint, and, in turn, inhibit excitatory LH neurons. As a result, the RVM neurons downstream of LH are disengaged when the mice try to escape, thus suppressing nociception. Next, our data indicate that the efforts to escape are communicated by the lateral periaqueductal gray (lPAG) to the LS and activation of the upstream lPAG→LS circuit phenocopies LS→LH activation and results in analgesia. Thus, we have revealed a poly-synaptic pathway that can transform escape behavior in mice under restraint to acute stress and resultant analgesia.

Introduction

Descending modulation of pain is the phenomenon through which the brain imparts control over somatosensory information processing in the spinal cord. Forebrain and midbrain regions encoding internal states such as stress and hunger can harness the brainstem circuits that communicate with spinal cord neurons to alleviate pain [1]. Such analgesic mechanisms are critical since they prepare animals and humans to cope actively with stressors or enable them to meet their physiological needs on time. Moreover, harnessing the underlying modulatory mechanisms may lead us to novel therapeutic approaches for pain. Stress-induced analgesia (SIA) is one such incidence where an acute stressor, such as physical restraint, can suppress pain. However, the neural mechanisms that facilitate SIA remain poorly understood.

Experiments involving human subjects in the 1950s and 1960s have shown that direct electrical stimulation of the lateral septum (LS) has anti-nociceptive [2,3] effects. Similarly, in rats, LS activation has been shown to suppress behavioral responses to sustained noxious stimuli such as intraplantar injections of formalin [4]. Further, septum inactivation or lesion renders rats hypersensitive to sensory stimuli, and as a result, they display exaggerated stimulus-driven defensive responses [5,6]. Despite these convincing leads indicating the involvement of LS neurons in the processing of noxious somatosensory stimuli, mechanistic investigation of the role of LS in nociception remains scarce. Classical studies involving lesions to lateral parts of the septal nucleus (LS) resulted in a phenomenon known as septal rage, which leads to heightened defensive responses against non-threatening stimuli, indicative of increased levels stress and anxiety [78]. Interestingly, LS is key in sensing acute stress and instrumental in stress-induced fear and anxiety [9–1112]. This involvement of the LS in acute stress-induced anxiety is reflected in behavioral phenotypes and in the elevated levels of blood corticosterone [13]. Taken together, LS neurons were shown independently to mediate the effects of both nocifensive behaviors and acute stress. However, the role of LS neurons in pain modulation in the event of an ongoing stressful stimulus remains unexplored. Hence, we hypothesized that the LS might play a facilitatory role in SIA.

The LS neurons communicate primarily through their inhibitory neurotransmitters and have prominent projections to diverse hypothalamic areas [9]. Of note are the projections to the lateral hypothalamus (LH). LH neurons have strong connections to the pain-modulatory nuclei in the brainstem, such as the rostral ventromedial medulla (RVM) and the lateral parabrachial nuclei (LPBN). In addition, recent studies have reported LH neurons to be able to sense noxious stimuli and suppress pain[14,15], and specifically, the projections to the RVM were shown to have anti-nociceptive effects[16–20]. Thus, we reasoned that the LS→LH circuitry, through downstream neurons in the RVM, may mediate SIA.

One commonly used laboratory model of acute SIA in animals is restraining (acute restraint stress or ARS) mice or rats in inescapable tubes or chambers. The stress is induced by the rodents' repeated efforts to escape and is a part of the repertoire of innate mechanisms which enable animals to evade stressors. Thus, LS→LH circuitry may potentially encode the intermittent escape responses in mice under restraint, culminating in acute stress and eventual SIA. These signals may be derived from escape circuits housed in the midbrain nuclei such as

the lateral periaqueductal gray (lPAG). The lPAG is known to be involved in active coping behavioral responses to stress[21]. The neurons in the lPAG in contrast to passive coping neurons in the lPAG, encode active coping behaviors in response to threats or stressors, such as escape in response to physical restraint [21].

Here, we have explored the mechanisms through which restraint stress-responsive LS neurons recruit downstream circuits to provide pain relief. Taking advantage of the recently developed anterograde trans-synaptic and retrogradely transporting viral genetic tools for anatomic circuit mapping, we have traced a pathway that originates in the brainstem lPAG, routes through the LS, and LH while finally terminating onto the spinally-projecting RVM neurons. Optogenetic and chemogenetic manipulations of the activity of each node of this pathway informed us on how they play interdependent roles in transforming restrain-induced stress into the suppression of acute and chronic inflammatory thermal pain. Notably, fiber photometry recordings from the involved nuclei shed light on how the neurons in the lPAG and LS sense the inability to escape restraint and suppress downstream LH and RVM neurons to facilitate SIA. Taken together, our data propose a mechanism that can explain how ARS can suppress pain and provides leads to gaining an understanding of how the circuitries dedicated to detecting stress can interface with the ones built for modulating pain.

Results

Struggle to escape during acute restraint is encoded by the LS neurons

To test if acute restraint stress (ARS) activates LS neurons, we induced ARS by restraining mice in a falcon tube for an hour [22] and probed the expression of c-Fos, a molecular proxy for neural activation in the lateral septum (LS) [23]. Mice exposed to ARS showed increased cFos immunoreactivity in the LS compared to controls, suggesting that (Figure 1A-C; S1A, B) the LS may mediate acute stress. This finding is consistent with previous studies that observed robust cFos expression in the LS in response to ARS [24,25]. Next, we sought to determine if the activity of LS neurons corresponded with the events of struggle to escape during ARS. This was important because LS neurons are known to be engaged during active escape attempts, and ARS is induced due to the inability of the mice to escape the restraint [24]. To that end, since most LS neurons are inhibitory (Figure 1D)[9], we expressed the genetically encoded fluorescent calcium sensor, GCaMP6s in LS neurons [26] under the inhibitory neuron-specific Gad67 promoter ($LS^{Gad67\text{-}GCaMP6s}$) (Figure 1E, F). We recorded calcium transients with a fiber photometry system [27] in mice undergoing ARS, and as expected, we observed spontaneous transients in the LS neurons of mice expressing GCaMP6s but not GFP (Figure 1G). Notably, in mice under ARS, $LS^{Gad67\text{-}GCaMP6s}$ neurons were active only when they struggled and not when they freely ran in their home cages (Figure 1H, I). Thus, suggesting that the increased neural activity during the struggle in mice under ARS was not simply due to the increased physical activity but to the need and inability to escape restraint. Similarly, we restrained mice acutely by hand, and $LS^{Gad67\text{-}GCaMP6s}$ neurons became active during the initial immobilization phase while the mice struggled (Figure 1K, L). The activity was reduced once the mice were physically restrained and were unable to move. $LS^{Gad67\text{-}GCaMP6s}$ neurons became active again when the experimenter loosened the grip and set the mice free (Figure 1K, L). Thus, in agreement with the previous result, the $LS^{Gad67\text{-}GCaMP6s}$ neurons were active when the mice actively struggled to escape acute restraint. Mice are stressed when they are actively hung by their tail [28], and we observed that the $LS^{Gad67\text{-}GCaMP6s}$ neurons are activated during the tail-hanging assay (Figure 1M, N). Next, we tested if the $LS^{Gad67\text{-}GCaMP6s}$ neurons respond to noxious thermal stimuli. On the hot-plate test [29], a commonly used behavioral assay to expose rodents to noxious hot surface temperatures (52^{o}C for 20 seconds) and measure their responses, $LS^{Gad67\text{-}GCaMP6s}$ neurons were not activated (Figure 1O-R). In addition, when we induced persistent peripheral thermal hyperalgesia by injecting intra-plantar complete Freund's adjuvant (CFA) [30,31] in mice, the $LS^{Gad67\text{-}GCaMP6s}$ neurons did not respond on the hot-plate test (Figure 1S-V). Thus, $LS^{Gad67\text{-}GCaMP6s}$ neurons are preferentially tuned to physical restraint stress, not to noxious thermal stimuli.

LS neurons play a critical role in ARS-induced analgesia

Since ARS provides short-term analgesia [32] and engages LS neurons, we hypothesized that artificial stimulation of LS neurons should be sufficient to cause acute stress and to facilitate pain suppression. To test this, we transiently activated the inhibitory LS neurons by expressing hM3Dq, a Gq-coupled DREADD with a similar genetic strategy as used in Figure 1E [33,34] ($LS^{Gad67\text{-}hM3Dq}$) (Figure 2A). In the control mice, we expressed the fluorescent protein tdTomato ($LS^{Gad67\text{-}tdTomato}$). Intraperitoneal (i.p.) administration of the DREADD ligand, Deschloroclozapine (DCZ) [35], in the $LS^{Gad67\text{-}hM3Dq}$ neurons activated these neurons, which were substantiated by the increase in cFos protein expression (Figure 2B). Desclozapine-driven increase in cFos

expression was not noticed in the $LS^{Gad67\text{-}tdTomato}$ neurons (Figure 2B). Chemogenetic activation of the LS resulted in increased serum corticosterone levels (Figure S1C), and led the mice to spend a longer time on the unlit side of the light-dark box (Figure S1D, E).
These observations indicated that the LS neurons are sufficient to induce heightened stress responses and anxiety-like behaviors. Next, we tested the effect of $LS^{Gad67\text{-}hM3Dq}$ stimulation on the behavioral responses to noxious thermal stimuli. To that end, we used the tail-flick and the hot-plate tests to measure the spinal and supraspinal responses to thermal noxious stimuli, respectively [36,37]. In the tail-flick test, radiant heat is focused on the tail leading to a spinal cord-mediated reflexive withdrawal of the tail. While on the hot-plate test, mice respond with shakes, licks, and jumps in response to noxious heat. We used the CD1-inbred strain of mice for our behavioral experiments, and on the hot-plate test at 52ºC for 1 minute, CD1 mice were inconsistent in their jumping responses (Figure S1J). Hence, we used shakes and licks as the behavioral readouts for the hot-plate test. Compared to saline, i.p. DCZ in the $LS^{Gad67\text{-}hM3Dq}$ mice increased the reaction latency on the tail-flick test (Figure 2G). DCZ did not alter tail-flick latency in the control $LS^{Gad67\text{-}tdTomato}$ mice (Figure 2C). When the LS neurons were activated, the number of licks on the hot-plate test decreased, while the latency to lick increased (Figure 2H). Next, we tested the effect of LS activation in mice with thermal hypersensitivity due to chronic inflammation. We injected chronic Freund's adjuvant (CFA) in the paw (intraplantar or i.pl.) to induce peripheral inflammation and thermal hyperalgesia. We confirmed the hyperalgesia in CD1 mice injected with i.pl. CFA by testing them on a gradient thermal plate test where the surface temperature was increased from 32 to 52ºC over 6 minutes (Figure S1F-I). I.pl. CFA and not saline injection increased the number of licks, and lowered the temperature at which the licks were initiated. The hypersensitivity did not affect the number of shakes but reduced the threshold temperature at which mice started shaking their paws (Figure S1F-I). Strikingly, LS^{Gad67} stimulation was sufficient to suppress licking in mice with i.pl. CFA and increase the latency to lick (Figure 2H). In complementary experiments, we evaluated the effect of optogenetic stimulation of LS^{Gad67} neurons on thresholds for noxious thermal stimuli. In agreement with our chemogenetic activation studies (Figure 2A-H), optogenetic stimulation [38] of the LS neurons by the expression of ChR2-YFP [39] under the Gad67 promoter ($LS^{Gad67\text{-}ChR2}$) (Figure 2M, N) and illumination by blue light via optic fiber cannulae was sufficient to cause analgesia (Figure 2O, P). Control mice expressing GFP under the Gad67 promoter in the LS ($LS^{Gad67\text{-}GFP}$) (Figure 2I, J) neurons showed no difference in heat thresholds or incidences of nocifensive behaviors upon blue light illumination. (Figure 2K, L). The LS optogenetic activation-induced analgesia was sustained when mice were challenged with i.pl. CFA-induced peripheral inflammation. To summarize, transient excitation of LS neurons resulted in stress-induced anxiety, higher serum corticosterone levels, and analgesia.

Next, we tested if the LS^{Gad67} neurons are required for ARS-induced analgesia. We silenced the LS^{Gad67} neurons by expressing tetanus toxin light chain protein fused with GFP (TetTox-GFP) [40,41]($LS^{Gad67\text{-}TetToxGFP}$) (Figure 3A) and tested if the silencing would interfere with the ARS-induced analgesia. Neuronal expression of TetTox impairs spike-evoked neurotransmitter release [42,43]. We ascertained TetTox mediated blockade of synaptic release from the LS^{Gad67} neurons by co-expressing TetTox-GFP, and hM3Dq-mCherry or GFP, and hM3Dq-mCherry as controls (Figure S2A). I.p. DCZ in the mice expressing GFP and hM3Dq in the LS and not in the mice expressing TetTox-GFP and hM3Dq-mCherry increased the

threshold for reaction in the tail-flick test (Figure S2B). Thus, TetTox expression in the LS^{Gad67} neurons was sufficient to impede the synaptic communication between the LS^{Gad67} neurons and their post-synaptic targets and resulted in the loss of analgesia observed otherwise by the chemogenetic activation of the LS^{Gad67} neurons (Figure 2G). Next, we induced ARS by restraining the mice in ventilated falcon tubes for 60 minutes (Figure 1A) [24,44]. We ascertained that our ARS paradigm induced stress by measuring the blood corticosterone levels (Figure S1C), and stress induced-anxiety like behavior (Figure S1D, E). Further, ARS-induced analgesia lasted for around 30 minutes after the mice were released from the tube restraint (Figure S2C). Notably, the ARS induced analgesia and analgesia induced by 30 minutes of optogenetic stimulation of $LS^{Gad67\text{-}ChR2}$ neurons were comparable (Figure S2C, D). When we tested the effect of ARS on tail-flick latency in the $LS^{Gad67\text{-}TetToxGFP}$ mice and the control $LS^{Gad67\text{-}GFP}$ mice, we observed that the silencing of the synaptic transmission in LS neurons abolished ARS-induced analgesia (Figure 3C, G). Similarly, ARS reduced the number of licks and increased the latency to lick in control $LS^{Gad67\text{-}GFP}$ mice on the hot-plate test, while in the $LS^{Gad67\text{-}TetToxGFP}$ mice, ARS did not have any analgesic effect (Figure 3D, H). In complementary experiments, we expressed the inhibitory opsin, halorhodopsin (eNpHR3.0) [45] in the LS^{Gad67} ($LS^{Gad67\text{-}eNpHR3.0\text{-}YFP}$) neurons to test if acute silencing of the LS^{Gad67} neurons will interfere with ARS-induced analgesia. In agreement with the TetTox mediated silencing experiments (Figure 3A-H), shining yellow light on the $LS^{Gad67\text{-}eNpHR3.0\text{-}YFP}$ neurons through fiber optic cannulae impaired ARS-induced analgesia (Figure 3I-L). In the control mice, LS^{Gad67} neurons expressed GFP ($LS^{Gad67\text{-}GFP}$), and ARS-induced analgesia was observed (Figure 3O, P) in the presence or absence of yellow light. Further, optogenetic silencing of the LS^{Gad67} neurons was sufficient to reverse the ARS-induced analgesia seen in mice with thermal hyperalgesia and inflammation (Figure S3I, J). Our data demonstrate that chronic (TetTox) and acute inhibition (eNpHR3.0) of LS^{Gad67} neurons impede ARS-induced analgesia to noxious thermal stimuli, suggesting that the LS is required for bringing about ARS-induced analgesia.

LS neurons synapse onto the Vglut2-expressing LH neurons

Next, we sought to determine the post-synaptic neurons through which LS neurons facilitate ARS-induced analgesia. To address this, we mapped the axonal targets of LS^{Gad67} neurons by labelling these neurons with cell-filing GFP ($LS^{Gad67\text{-}GFP}$). In agreement with previous reports, we observed $LS^{Gad67\text{-}GFP}$ axon terminals in the lateral hypothalamus (LH), the habenula (Hb), and the hippocampus (Figure 4A, B; Figure S3A) [46,47]. Given that LH neurons can determine nociceptive thresholds [14,48] and the LH has direct access to pain-modulatory areas in the brain stem, such as the periaqueductal gray (PAG), the lateral parabrachial nucleus (LPBN), and the rostral ventromedial medulla (RVM) [14], we hypothesized that LS neurons may exert their analgesic effect through neurons in the LH. To confirm that the axonal terminals of the LS neurons at the targets form functional synapses with the neurons in the LH, we labeled the axon terminals of LS^{Gad67} neurons with synaptophysin fused with the red fluorescent protein ruby ($LS^{Gad67\text{-}SynRuby}$) (Figure 4C) and found SynRuby puncta in all LS^{Gad67} axonal targets, including the LH (Figure 4D), suggesting that LS neurons form functional synapses onto LH neurons ($LH_{post\text{-}LS}$)

Next, we sought to determine if LH neurons receiving inputs from LS are excitatory or inhibitory, given that LH is composed of both excitatory and inhibitory neurons, which express

VGlut2 and VGat, respectively (Figure S3B, C). VGlut2-expressing neurons are relatively fewer in number (Figure S3B, C) and have recently been implicated in pain modulation [14]. To test if VGlut2+ LH neurons receive direct input from LS^{Gad67} neurons, we took three complementary approaches. First, we injected AAV1-FlpO with anterograde transsynaptic transmission properties (AAV1-hSyn-FlpO or Transyn-FlpO) [49–51] in the LS of VGlut2-Cre transgenic mice (Figure 4E, F). Simultaneously, we injected DIO-GFP and fDIO-tdTomato in the LH of the same mice (Figure 4E, F). We found that 34.2 ± 9.6 % (n = 8 sections, 3 mice) tdTomato expressing cells ($LH_{post\text{-}LS}$) were GFP +ve, indicative of their excitatory status. Second, we delivered anterograde transsynaptic Cre (AAV1-hSyn-Cre or Transyn-Cre) in the LS of Rosa26-LSL-tdTomato transgenic mice to label the $LH_{post\text{-}LS}$ neurons with tdTomato and performed multiplex fluorescent in-situ hybridization for VGlut2 and tdTomato mRNA in the LH (Figure 4G, H). We found that 28.5 ± 11.2 % (n = 12 sections, 2 mice) tdTomato neurons colocalized with VGlut2. Third, we labeled the synaptic terminals of LS^{Gad67} neurons and post-synaptic densities of LH^{VGlut2} neurons by expressing synaptophysin-fused GFP (SynGFP) in the LS^{Gad67} neurons and Cre-dependent inhibitory post-synaptic protein, Gephryn fused with red fluorescent protein tagRFP (DIO-GephryntagRFP)[5253,54] in the LH (Figure 4I) of VGlut2-Cre mice, respectively. Here, we noticed close apposition of green synaptophysin and red gephyrin puncta in the LH (Figure 4J), suggesting that LS^{Gad67} neurons make synaptic connections onto VGlut2 neurons in the LH ($LH_{post\text{-}LS}^{VGlut2}$). Overall, these results suggest that inhibitory LS axons synaptically target the excitatory populations of LH neurons. Since parvalbumin (PV) labels a subset of excitatory neurons in the LH and PV-expressing neurons in the LH have been shown to be antinociceptive [14], we tested if $LH_{post\text{-}LS}$ neurons colocalize with PV-expressing cells, and found little to no overlap between the two populations (Figure S3D).

Next, we reasoned that if $LH_{post\text{-}LS}$ neurons are inhibited by LS^{Gad67} neurons, then $LH_{post\text{-}LS}$ neurons must be disengaged when mice undergo acute stress. To test this, we recorded calcium transients from $LH_{post\text{-}LS}$ neurons as mice underwent ARS and were exposed to noxious thermal stimuli. To that end, we labeled $LH_{post\text{-}LS}$ neurons with GCaMP6s ($LH_{post\text{-}LS}^{GCaMP6s}$) (Figure 4K, L), using an intersectional transsynaptic strategy similar to the one in Figure 4G. Surprisingly, fiber photometry recordings showed that $LH_{post\text{-}LS}^{GCaMP6s}$ neurons respond to acute stress caused by physical restraint and tail hanging (Figure 4 M, N; Figure SE-H). In addition, like LS^{Gad67} neurons (Figure 1O-V), $LH_{post\text{-}LS}^{GCaMP6s}$ neurons were not engaged by noxious thermal stimuli. Notably, $LH_{post\text{-}LS}^{GCaMP6s}$ neurons differed in their activity from the $LS^{Gad67\text{-}GCaMP6s}$ neurons in one aspect — while mice struggled in the ARS assay, $LS^{Gad67\text{-}GCaMP6s}$ neurons were active for the entire duration of the physical struggle (up to 10 seconds) (Figure 4N) to escape, $LH_{post\text{-}LS}^{GCaMP6s}$ neurons were active only during the initial phase of the struggle (1-3 seconds) (Figure 4M). This indicates that activity of pre-synaptic LS and post-synaptic $LH_{post\text{-}LS}$ neurons increase in a coordinated manner at the onset of struggle in mice undergoing ARS-assay. However, after the initial activity, LH_{LS} neurons can potentially be suppressed by inhibitory LS inputs. Taken together, these data suggest that acute stress inhibits a sub-population of excitatory neurons in the LH that are post-synaptic to inhibitory LS neurons.

LS-LH circuitry is sufficient and necessary for ARS-induced analgesia

Next, we tested if activation of the LS→LH circuitry can facilitate ARS-induced analgesia. To that end, we selectively stimulated the axon terminals of the LS^{Gad67} neurons in the LH by expressing ChR2 in the LS ($LS^{Gad67\text{-}ChR2}$) and shining blue light on the terminals at LH through fiber optic cannulae (Figure 5A). Selective activation of the $LS^{Gad67\text{-}ChR2}$ terminals in the LH resulted in increased latency on the tail-flick assay and a reduced number of licks with an increased threshold on the hot-plate assay (Figure 5B, C), suggestive of analgesia. The analgesic effect of LS^{Gad67} terminal activation was preserved even in hypersensitive mice challenged with i.pl. CFA. These observations were similar to the results from the experiments where the cell bodies of $LS^{Gad67\text{-}ChR2}$ neurons were stimulated (Figure 2O, P). Taken together, these results suggest that stimulating LS^{Gad67} cell bodies or their axon terminals in the LH is sufficient to cause analgesia. In complementary experiments, we chemogenetically activated LS^{Gad67} terminals in the LH. To that end, we devised a novel microparticle (MP)-based delivery system [55,56] for CNO (for the MP-based delivery system, hM3Dq agonist CNO was used due to greater hydrophobicity, which is essential for MP packaging, compared to DCZ), which can be implanted specifically in the LH where LS neurons terminate (Figure S4 A-C). Compared to the widely-used method for in-vivo drug delivery at deep brain nuclei through cannulae [57,58], our PLGA (poly-DL-lactic-co-glycolic) microparticle (MP-CNO) based system (see methods) can serve as a stable, cost-effective, non-invasive, site-specific, and sustained method for CNO delivery. To demonstrate the efficacy of the MP-CNO, we stereotaxically implanted MP-CNO in the LS (Figure S4D, G) of $LS^{Gad67\text{-}hM3Dq}$ or $LS^{Gad67\text{-}tdTomato}$ (control) mice. In the $LS^{Gad67\text{-}hM3Dq}$ mice, MP-CNO was analgesic, and the effects were pronounced (Figure S 4E, F, H, I) between 48-96 hours of delivery. Remarkably, the MP-CNO-induced analgesia was comparable to that of i.p. CNO administration (Figure S4 H, I). Finally, we delivered MP-CNO in the LH of $LS^{Gad67\text{-}hM3Dq}$ mice for terminal activation and observed increased tail-flick thresholds, fewer licks, and higher lick thresholds (Figure S J-L). Thus, our acute optogenetic and chronic chemogenetic axon terminal activation experiments demonstrate that LS neurons could bring about analgesia through their projections to the LH.

Next, we chemogenetically stimulated the LS neurons whose axon terminals arborize and synapse onto the LH neurons ($LS_{pre\text{-}LH}$). To that end, we injected retrogradely transporting AAV (AAVRetro-Cre) in the LH and DIO-hM3Dq-mCherry in the LS. This intersectional genetic strategy facilitated excitatory DREADD expression exclusively in $LS_{pre\text{-}LH}$ neurons ($LS_{pre\text{-}LH}^{hM3Dq\text{-}mCherry}$) (Figure 5G). Controls expressed tdTomato in $LS_{pre\text{-}LH}$ neurons ($LS_{pre\text{-}LH}^{tdTomato}$). i.p administration of DCZ in the $LS_{pre\text{-}LH}^{hM3Dq\text{-}mCherry}$ and not the $LS_{pre\text{-}LH}^{tdTomato}$ mice was analgesic (Figure 5E, F, H, I), indicating that activation of a specific subset of LS neurons ($LS_{pre\text{-}LH}$) is sufficient for altering thermal nociception in mice. In the following experiments, we asked what the effect of chemogenetic activation of the LH neurons downstream of LS ($LH_{post\text{-}LS}$) on thermal nociceptive thresholds would be. To address this, we chemogenetically activated $LH_{post\text{-}LS}$ neurons by injecting AAVTrans-Cre in the LS and AAV-DIO-hM3Dq-mCherry in the LH (Figure 5M). Controls expressed tdTomato in $LH_{post\text{-}LS}$ neurons (Figure 5J). I.p. administration of DCZ in mice expressing hM3Dq and not tdTomato in $LH_{post\text{-}LS}$ neurons reduced the latency to react on the tail-flick assay, increased the number of licks, and decreased the latency to lick on the hot-plate test (Figure 5K, L, N, O). Intriguingly, our data suggest that when activated, LS^{Gad67} neurons inhibit LH neurons to cause analgesia, and so when $LH_{post\text{-}LS}$ neurons are artificially activated, it has the

opposite effect on nocifensive behaviors and leads to hyperalgesia. In addition, given that LS neurons project to the Hb (Figure 4B) and Hb neurons have been shown to have anti-nociceptive effects [59], we asked if activating Hb neurons post-synaptic to LS ($Hb_{post\text{-}LS}$) can alter thermal pain thresholds. We chemogenetically activated $Hb_{post\text{-}LS}$ neurons by injecting AAVTrans-Cre in the LS and DIO-hM3Dq-mCherry in the Hb ($Hb_{post\text{-}LS}^{hM3Dq}$) and administering DCZ intraperitoneally (Figure 5P). Saline-treated $Hb_{post\text{-}LS}^{hM3Dq}$ mice as served controls. However, DCZ or saline in mice with hM3Dq in the $Hb_{post\text{-}LS}$ neurons did not alter pain thresholds (Figure Q, R). Further, we tested the effects of silencing the $LH_{post\text{-}LS}$ neurons on ARS-induced SIA (Figure 5 S-X). Compared to controls (GFP), TetTox mediated $LH_{post\text{-}LS}$ silencing abolished SIA. In summary, the $LH_{post\text{-}LS}$ neurons are functionally downstream of LS^{Gad67} neurons, and simultaneous transient activation has identical effects on nociceptive thresholds under acute and chronic inflammatory conditions.

LS-LH circuitry induces analgesia through RVM and downstream spinal neurons

How do $LH_{post\text{-}LS}$ neurons facilitate ARS-induced analgesia? To answer this question, we mapped the projections of the $LH_{post\text{-}LS}$ neurons. Expression of GFP in the $LH_{post\text{-}LS}$ neurons, labeled axon-terminals in the lateral parabrachial nucleus (LPBN), and the rostral ventromedial medulla (RVM) (Figure 6 A-C). In previous studies, activation or silencing of LPBN neurons did not alter the reflexive withdrawal thresholds or coping responses, such as licks in response to noxious thermal stimuli [52,60,61]. However, RVM neurons are known to modulate pain bi-directionally [62,63]. Importantly, stress-induced analgesia is opioid-dependent [64–66], and RVM is a major substrate for endogenous opioids [62]. Further, simultaneous administration of mu-opioid receptor antagonist naltrexone and DCZ in $LS^{Gad67\text{-}hM3Dq}$ mice blocked LS activation-induced analgesia (Figure S5 I, J). Thus, we reasoned that the projections of the $LH_{post\text{-}LS}$ neurons synapse onto RVM neurons and facilitate ARS-induced analgesia. To that end, first, we sought to establish the anatomical location and projections of the RVM neurons ($RVM_{post\text{-}LH}$) — that are post-synaptic to the $LH_{post\text{-}LS}$ neurons. We labeled the $RVM_{post\text{-}LH}$ neurons with GFP (Figure 6 D) and SynRuby (Figure S5 A-C) separately, using the anterograde intersectional viral genetic strategy used before (AAVTrans-Cre in LH; DIO-GFP or DIO-SynRuby in RVM). We observed that the cell bodies of the $RVM_{post\text{-}LH}$ neurons were distributed in the midline area (Figure 6E, S5B) of the medulla. We noticed abundant axon terminals of $RVM_{post\text{-}LH}$ neurons in the LH (Figure S5C), PAG (not shown), and projections in the deeper layers (VI/ VII) in the lumbar spinal cord (Figure 6F, S5D). Thus, this implies that the $RVM_{post\text{-}LH}$ neurons may modulate nociceptive thresholds through their local synaptic connections within the RVM, recurrent connections with the PAG, or direct interactions with spinal cord neurons. Second, using the monosynaptic retrograde rabies tracing technique [67,68], we determined if the $RVM_{post\text{-}LH}$ neurons are the direct post-synaptic partners of the $LH_{post\text{-}LS}$ neurons. We expressed G and TVA-GFP proteins in the $LH_{post\text{-}LS}$ neurons (AAVTrans-Cre in LS; DIO-G; DIO-TVA-GFP in LH) and injected delG-Rabies-mCherry in the RVM (Figure 6G). As expected, we observed the starter cells that co-expressed TVA-GFP ($LH_{post\text{-}LS}$) and delG-Rabies-mCherry (retrogradely transported from the RVM; $LH_{pre\text{-}RVM}$) in the LH (Figure 6H). Remarkably, retrogradely transported Rabies-mCherry was found in the LS neurons (Figure 6H). Indicating that the LS neurons are directly upstream of the RVM projecting LH neurons. Third, in a complementary approach, we took advantage of the GRASP synaptic labeling strategy [69], where pre-synaptic neurons expressed

one-half of the GFP protein, and the post-synaptic neurons express the other half. At the functional synapses between the two GFP-subunit expressing neurons, GFP is reconstituted and can be visualized through a fluorescent microscope. In our experiments, we injected the Pre-GRASP in the LS, fDIO-Post-GRASP in the LH, and AAVRetro-FlpO in the RVM (Figure 6I) of the same mice. Simultaneous injection of the three AAVs successfully labeled the synapses between the LS and $LH_{pre\text{-}RVM}$ neurons with GFP in the LH (Figure 6J). Thus, demonstrating that the LS neurons make functional synaptic connections with $LH_{pre\text{-}RVM}$ neurons.

Next, we sought to understand how the $RVM_{post\text{-}LH}$ neurons encode ARS and noxious thermal stimuli, and thus, we performed fiber photometry recordings from the GCaMP6s expressing $RVM_{post\text{-}LH}$ neurons ($RVM_{post\text{-}LH\text{-}GCaMP6s}$) (Figure 6K, L). Calcium transients in the $RVM_{post\text{-}LH}$ neurons increased spontaneously when mice were subjected to ARS (Figure 6M). However, when the mice struggled under restraint, $RVM_{post\text{-}LH}$ neuronal activity was suppressed (Figure 6M, N). The activity of the $RVM_{post\text{-}LH\text{-}GCaMP6s}$ neurons increased when the mice shook or licked their paws on the hot-plate test (Figure 6O). Notably, the rise in activity of the $RVM_{post\text{-}LH}$ neurons preceded the licks and shakes, indicating a facilitatory role of these neurons in nocifensive behaviors. The facilitatory pro-nociceptive population of RVM neurons is otherwise known as ON-cells [70,71] In summary, $RVM_{post\text{-}LH}$ neurons are pro-nociceptive and likely ON cells. They are activated by acute stress and suppressed when the mice struggle to escape stress-causing restraint.

To further establish that the $RVM_{post\text{-}LH}$ neurons are ON cells, we chemogenetically activated the $RVM_{post\text{-}LH}$ neurons (Figure 7 A-H). Mice expressing hM3Dq and not tdTomato in the $RVM_{post\text{-}LH}$ responded with licks and shakes on the hot-plate test with lower latency when i.p. DCZ was administered (Figure 7 C, D, G, H). The number of licks on the hot-plate test was higher when $RVM_{post\text{-}LH}$ neurons were activated, but the number of shakes was lower (Figure 7H). The reduction in shakes might be due to the higher number of licks in the restricted time the mice were allowed on the hot plate. Contrary to $RVM_{post\text{-}LH}$ activation, when we chemogenetically and optogenetically silenced the $RVM_{post\text{-}LH}$ neurons (Figure 7 I-L; Q-X), the number of licks on the hot-plate test was reduced, and the latency to lick and tail-flick was increased. These findings agree with our hypothesis that the activated LS neurons inhibit $LH_{post\text{-}LS}$ neurons, which in turn deactivates $RVM_{post\text{-}LH}$ cells providing analgesia. Moreover, the observation (Figure 7M, N) that silencing bi-lateral LPBN neurons post-synaptic to LH (Figure O, P) did not affect mouse responses on hot-plate and tail-flick tests confirmed LH-RVM connections primarily mediate the anti-nociceptive effects of $LH_{post\text{-}LS}$ neurons.

Recent observations indicate that the pro-nociceptive ON cells in the RVM can be either excitatory or inhibitory [72]. Activating the excitatory ON cells results in hypersensitivity to noxious stimuli, whereas inhibiting the same neurons results in analgesia [72]. Since the chemogenetic activation of the pro-nociceptive $RVM_{post\text{-}LH}$ neurons resulted in thermal hyperalgesia and inhibition leading to pain suppression, we hypothesized that the $RVM_{post\text{-}LH}$ neurons are excitatory. Thus, to test our hypothesis, we expressed Syn-GFP in the LH of VGlut2-Cre mice, and PSD95-tagRFP (Figure S5E), in the RVM of the same mice. When we visualized the RVM with confocal and super-resolution microscopy (Figure S5 F-H), we found close apposition between the GFP-expressing pre-synaptic terminals and tagRFP-expressing VGlut2 expressing RVM neurons. Thus, we concluded that the excitatory LH neurons impinge upon the excitatory RVM-ON neurons to facilitate ARS-induced analgesia.

PAG informs LS of the restraint-induced struggle

Fiber photometry recordings from the LS, downstream $LH_{post\text{-}LS,}$ and $RVM_{post\text{-}LH}$ neurons indicate that, during ARS, this multi-synaptic circuitry is acutely tuned to the efforts to escape (Figure 1I; 4M, N; 6M-O). Thus, we wondered where the escape signals that are communicated to the LS originate. To that end, to identify the inputs to the LS across the brain, we injected retrogradely transporting nuclear-tagged mCherry fluorescent protein (nls-mCherry) [73] in the LS (Figure 8A). We found nls-mCherry expressing cells in the hippocampus (data not shown), the LH, and the lPAG (Figure 8B). The projections from the LH and lPAG to the LS were observed before in unbiased brain-wide input mapping studies done at the LS in mice [46] and functional lesion studies [73]. Neurons in the lPAG are known to mediate and, in particular, to initiate the escape responses to aversive stimuli [21,74–76]. Hence, we posited that the lPAG might inform LS neurons of the efforts to escape while the mice are under restraint, thus facilitating stress-induced analgesia through the downstream LH neurons. We sought to determine if the LS (LSpost-lPAG) neurons that receive inputs from the lPAG also project to the LH. To that end, we took two complementary approaches. In the first, we injected AAV-TransCre in the lPAG, intersected in the LS with DIO-GFP, and observed axon terminals in the LH (Figure 8C, D; S6 A, B). Simultaneously, we labeled the LS with tagRFP. Remarkably, we found that LS axon terminals are spread across the hypothalamus. However, $LS_{post\text{-}lPAG}$ neuron terminals are concentrated at the LH (Figure 8C, D; S6 A, B). Indicating that the $LS_{post\text{-}lPAG}$ is a fraction of the LS projections to the LH and likely performs specific roles. Second, we performed a monosynaptic rabies tracing experiment by injecting AAVRetro-Cre in the LH and DIO-TVA-GFP, DIO-G, and delG-Rabies-mCherry in the LS (Figure 8E). This allowed us to reveal the pre-synaptic partners of the LS neurons that specific project to the LH. We observed delG-Rabies-mCherry labeling in neurons in the hippocampus, LH, and lPAG. Thus, concluding that the $LS_{pre\text{-}LH}$ neurons receive synaptic inputs from the lPAG. To test if lPAG neurons are functionally upstream of LS neurons, we expressed hM3Dq in the $LS_{post\text{-}lPAG}$ neurons by injecting AAVTrans-Cre in the lPAG and DIO-hM3Dq in the LS. DCZ-mediated chemogenetic activation of $LS_{post\text{-}lPAG}$ neurons decreased the number of licks and shakes on the hot-plate test (in contrast to saline-injected controls) while simultaneously increasing the latency (Figure 8H-L). The analgesic effects of activating the $LS_{post\text{-}lPAG}$ neurons persisted when mice were challenged with i.pl. CFA (Figure 8H-L). Thus as observed in the experiments where LS^{Gad67} or $LS_{pre\text{-}LH}$ neurons were chemogenetically activated (Figure 2G, H; 5H, I), $LS_{post\text{-}lPAG}$ stimulation resulted in thermal analgesia, indicating that lPAG neurons are functionally upstream of the LS→LH circuitry.

Moreover, lPAG neuronal population comprises excitatory and inhibitory neurons [77]. Since activation of the inhibitory neurons in the LS facilitates analgesia, the excitatory VGlut2-expressing lPAG projection neurons likely synapse onto LS neurons to mediate SIA. To test this, we labeled lPAG projection neurons with SynGFP by injecting AAV-DIO-GFP in the lPAG in VGlut2-Cre mice ($lPAG^{VGlut2}$) and DIO-PSD95-tagRFP under the Gad67 promoter in the LS (Figure S6E) . Since PSD95 is enriched in the dendrites of the excitatory synapses, the close apposition between the SynGFP and the PSD95-tagRFP in the LS neurons demonstrated synaptic connections between the lPAG and LS (Figure S6 D-F). Finally, we recorded the activity of $lPAG^{VGlut2}$ neurons in response to acute restraint (Figure 8 L-N). $lPAG^{VGlut2}$ neurons

were tuned to the efforts to escape while the mice were restrained, similar to their post-synaptic LS^{Gad67} neurons. When we calculated the area under the curve (AUC) of the Z-score of the recordings from the $lPAG^{VGlut2}$, LS, $LH_{post\text{-}LS}$, and $RVM_{post\text{-}LH}$ neurons while the mice struggled in the ARS assay, the data indicated that the $lPAG^{VGlut2}$ and LS activity increased while at the same time $LH_{post\text{-}LS}$, and $RVM_{post\text{-}LH}$ activity decreased (Figure 8N). Thus, the struggle to escape restraint engages lPAG excitatory neurons, activating $LS_{post\text{-}lPAG}$ inhibitory neurons. The activated inhibitory $LS_{post\text{-}lPAG}$ neurons silence excitatory $LH_{post\text{-}LS}$ neurons, which consequently disengages the pro-nociceptive $RVM_{post\text{-}LH}$ neurons to drive ARS-induced analgesia (Figure S6G).

Discussion

The lateral septum (LS) has been traditionally considered a key brain region for mediating stress responses [10,13,24,25]. However, the role of the LS in stress-induced analgesia (SIA) needs to be better understood. In this study, we have delineated the upstream and downstream partners of LS and elucidated the mechanisms through which LS neurons translate stress into pain suppression. We found that the LS neurons are specifically geared towards coping with stress and, through their connections with the spinal cord via the lateral hypothalamus (LH) and the rostral ventromedial medulla (RVM), inhibit responses to noxious stimuli. Additionally, our findings suggest that the brainstem lPAG neurons encode escape responses and transmit them to the LS. In conclusion, our study has comprehensively evaluated the involvement of crucial neural circuitries in SIA by anatomically tracing their anatomical connections, monitoring, and manipulating neural activity. This multidisciplinary approach has provided insights into SIA's previously unknown underlying mechanisms.

We wondered what the etiologically relevant function of SIA might be, evolutionarily what benefits SIA might provide, and how LS plays a role in it. SIA enables animals and humans to physiologically and behaviorally evade or cope with stressors in their immediate environment. When the perceived pain is attenuated, attention is drawn toward escaping the stressor. Several experiments support this view, including studies where rats were subjected to mild electric shocks from a floor plate in either an inescapable or an escapable chamber. It was observed that analgesia occurred when the rats could not escape the chamber after experiencing the electric shocks as opposed to when they could escape [78,79]. In line with these studies, we experimentally observed SIA only when mice were restrained for a sufficient amount of time (~1 hour) or when LS neurons were activated for ~30 mins (Figure S2C, D).

SIA can be particularly pertinent in individuals with chronic pain, where pathological pain can impede the ability to react to a stressor on time. Indeed, in our experiments, we observed that the LS-centric SIA circuitry is effective in suppressing hyperalgesia in mice with chronic inflammatory pain. Interestingly, contrary to our findings, a recent study have shown that the LS neurons promote both pain and anxiety [80]. The contradiction may be because the authors have primarily tested for mechanical sensitivity while we have focused on the thermal thresholds. In addition, the targeted coordinates for LS used in the study are medial compared to the ones to used in our study. However, as mentioned before, lesion studies in humans or animals have consistently indicated that the LS or medial septum stimulation is anti-nociceptive, irrespective of the nature of the noxious stimuli.

Early studies showed that SIA could either be opioid-dependent or independent [81]. Naltrexone administration blocked SIA in rats who had undergone electric shocks [82,83]. Surprisingly, it was found that acute stress can sequentially induce both opioid dependents as well as opioid-independent SIA [84]. Mutant mice without functional β-endorphin (endogenous ligand for the mu-opioid receptor, OPRM1) lacked opioid-dependent SIA (mild swim stress), however, they displayed opioid-independent SIA (cold-swim stress) [85]. Interestingly, opioid-dependent SIA was primarily induced when the animals underwent stress in inescapable chambers. Thus successful induction of SIA may depend on the mode of stress delivery, and the opioid dependence may be decided by the exposure time. Our data too suggests that LS-mediated ARS-induced analgesia is opioid dependent, as we found that SIA induced by LS activation is reversible by naltrexone administration (Figure S5I, J). Further, we show that RVM-

ON cells play a critical role in LS-mediated SIA. This observation is supported by a recent study that demonstrated the necessity of kappa-opioid receptors expressing RVM neurons in SIA[72]. Together, the restraint-induced silencing of LH excitatory neurons by LS may turn downstream mu-opioid receptor-expressing RVM-ON cells amenable to enkephalin and endorphin-mediated modulation and consequent analgesia.

In summary, our data suggest that ARS is initiated as escape responses in the midbrain, converted to stress in the downstream LS-LH circuitry, and promotes anti-nociception through their downstream $RVM_{post\text{-}LH}$ neurons (Figure S6G). Our anatomic labeling experiments (Figure 8A, B, E, F) retrogradely traced inputs to the LS from dlPAG and lPAG. However, few cells which were pre-synaptic to LH were found in the vlPAG. Here, we have used lPAG to refer to the neurons in both lPAG and vlPAG. We have refrained from directly stimulating the lPAG neurons since they are nociceptive and have access to the RVM [77,86]. We have primarily focused on thermal noxious stimuli that elicited defensive behaviors and inflammatory pain. Future studies can further elucidate how the circuits in focus here mediate mechanical pain behaviors and chronic neuropathic pain. Notably, prolonged exposure to stress can exacerbate pain [87], and it is necessary to understand how the LS-centric circuit presented here might intervene in pain-induced hyperalgesia.

Notably, LH neurons are known to respond to stress stimuli [88,89] and thus can cause SIA independently of LS. This is reflected in our results where we observed transient activation of $LH_{post\text{-}LS}$ neurons when the mice strugged in the ARS assay (Figure 4M). In addition to the excitatory projections tested here, there are inhibitory neurons in the LH that project to the PBN [90]. How both excitatory and inhibitory outputs from the LH can modulate responses to noxious stimuli remains to be investigated. In addition to the RVM and PBN, excitatory LH neurons project to the PAG and thereby may feed information into the PAG-RVM pain inhibitory circuits and modulate SIA [19,9119]. Decades of circuit tracing and functional anatomy studies have revealed synaptic targets of LH across the brain, including the LS[92]. Such bidirectional connections also exists between the RVM and LH, and exploring the roles of recurrent connections between LS-LH/ LH-RVM in stress-induced pain modulation will further delineate circuit mechanisms of SIA. We developed the microparticle-based CNO administration tool for projection-specific chronic DREADD ligand delivery. The same tool, by tweaking the release rates of the CNO, can be effectively used for chronic neuronal activation/silencing. Finally, the mechanistic interrogation of LS-centric SIA circuits has revealed a hypothalamic coordinate that effectively connects LS with RVM to influence nociceptive thresholds. We have primarily focused on thermal nociceptive thresholds, howebIt will be interesting to explore how LS-LH circuitry influences the effects of stress on other somatosensory modalities, such as itch.

Experimental Model and Subject Details

Mouse lines

Animal care and experimental procedures were performed following protocols approved by the CPSCEA at the Indian Institute of Science. The animals were housed at the Central Animal Facility under standard transgenic animal housing conditions Vglut2-Cre or Vglut2-ires-Cre or Slc17a6tm2(Cre) Lowl/J(Stock number 016963); Ai14 (B6;129S6-Gt(ROSA)26Sortm9(CAG-tdTomato)Hze/J (Stock No 007905) strains Jackson Laboratories, USA, were used.

Methods

Viral vectors and stereotaxic injections

Mice were anesthetized with 2% isoflurane/oxygen before and during the surgery. Craniotomy was performed at the marked point using a hand-held micro-drill (RWD). A Hamilton syringe (10 ul) with a glass pulled needle was used to infuse 300 nL of viral particles (1:1 in saline) at 100 nL/min. The following coordinates were used to introduce virus/dyes: LS- AP: +0.50, ML: + 0.25; DV: -2.50; LH- AP: -1.70, ML: ±1.00; DV: -5.15; RVM- AP: -5.80, ML: +0.25; DV: -5.25; PBNl- AP: -5.34, ML: ±1.00, DV: -3.15; lPAG- AP: -4.84, ML: ±0.5, DV: -2.75. Vectors used and sources: ssAAV-9/2-hGAD67-chl-icre-SV40p(A) (University of Zurich), pAAV5-hsyn-DIO-EGFP (Addgene), pAAV5-FLEX-tdTomato (Addgene), pENN.AAV5.hSyn.TurboRFP.WPRE.RBG (Addgene), pAAV5-hsyn-DIO-hM3D(Gq)-mCherry (Addgene), pAAV5-hsyn-DIO-hM4D(GI)-mCherry (Addgene), AAV9.syn.flex.GcaMP6s (Addgene), pAAV-Ef1a-DIO-eNPHR 3.0-EYFP (Addgene), pAAV-EF1a-double floxed-hChR2(H134R)-GFP-WPRE-HGHpA(Addgene), AAV1-hSyn-Cre.WPRE.hGH (Addgene), AAVretro-pmSyn1-EBFP-Cre (Donated by Ariel Levine, NIH), AAV retro-hSynapsin-Flpo (Donated by Ariel Levine, NIH), scAAV-1/2-hSyn1-FLPO-SV40p(A) (University of Zurcih), ssAAV-1/2-shortCAG-(pre)mGRASP-WPRE-SV40p(A) (University of Zurich), ssAAV-1/2-fDIO-(post)mGRASP_2A_tdTomato(University of Zurich), pAAV-Ef1a-DIO-tdTomato (Addgene), pAAV-hSyn-fDIO-hM3D(Gq)-mCherry-WPREpA (Addgene), ssAAV-9/2-hSyn1-chl-dlox-EGFP_2A_FLAG_TeTxLC(rev)-dFRT-WPRE-hGHp(A) (University of Zurich), AAVretro-hSyn-NLS-mCherry (Donated by Ariel Levine, NIH), AAV9-DIO-GephrynTagRFP (Donated by Mark Hoon, NIH), AAV9-DIO-PSD95-TagRFP (Donated by Mark Hoon, NIH)AAV5-hSyn-DIO-mSyp1_EGFP(University of Zurich). For rabies tracing experiments, rAAV5-EF1α-DIO-oRVG and rAAV5-EF1α-DIO-EGFP-T2A-TVA (BrainVTA) were injected first, followed by RV-EnvA-Delta G-dsRed (BrainVTA) after 2 weeks. Tissue was harvested after 1 week of rabies injection for histochemical analysis. Post-hoc histological examination of each injected mouse was used to confirm that viral-mediated expression was restricted to target nuclei.

Optogenetic and Photometry fiber implantation

Fiber optic cannula from RWD; Ø1.25 mm Ceramic Ferrule, 200 µm Core, 0.22 NA, L = 5 mm were implanted at AP: 0.50, ML: +0.25; DV: -2.50 in the LS and L= 7mm fibers were implanted at AP: -1.70, ML: ±1.00; DV: -5.15 in the LH, and AP: -5.80, ML: +0.25; DV: -5.25 in the RVM after AAV carrying GCamp6s, Chr2 or Halorhodopsin were infused. Animals were allowed to recover for at least 3 weeks before performing behavioral tests. Successful labeling

and fiber implantation were confirmed post hoc by staining for GFP/mCherry for viral expression and injury caused by the fiber for implantation. Animals with viral-mediated gene expression at the intended locations and fiber implantations, as observed in posthoc tests, were only included.

Behavioral assays

Behavioral assays for the same cohorts were handled by a single experimenter. Mice were habituated in their home cages for at least 30 min in the behavior room before experiments. An equal male-to-female ratio was maintained in every experimental cohort and condition unless otherwise stated. DCZ was diluted in saline and injected i.p. 15-20 minutes before behavioral experiments or histochemical analysis. Mice were injected with i.pl. CFA one day before the behavioral experiments to cause persistent inflammatory pain and thermal hypersensitivity. All the experiments were videotaped simultaneously with three wired cameras (Logitech) placed horizontally and scored offline post hoc manually. The programmable hot-plate with gradient function and tail flick analgesiometer were (Orchid Scientific, India) used according to the manufacturer's instructions. For optogenetic stimulations fiber-coupled laser (channelrhodopsin activation; RWD), fiber-coupled LEDs (for halorhodopsin stimulation; Prizmatix), were used. Prior to the behavioral testing the optic fibers were connected to the cannulae implanted in the mice brain. The animals were habituated for 30 minutes prior to the commencement of the experiments. The light-dark box tracking and estimations of the time-spent in either chamber were performed with DeepLabCut [93].

The Acute Restraint Stress Assay (ARS) was used to induce stress in the mice to test for analgesia. Mice were restrained for one hour in a ventilated falcon tube, followed by testing them for stress-related and noxious behaviors using the Light Dark Box Assay, the Hot Plate Assay, and the Tail Flick Assay.

Blood corticosterone levels were measured using the Mouse corticosterone ELISA kit (BIOLABS) by collecting blood from control wild-type mice, wild-type mice subjected to ARS, and $LS^{Gad67\text{-}hM3Dq}$ mice administered with DCZ.

The mice were subjected to four primary behavioral assays for the fiber photometry experiments. In the immobilization experiments, experimenter physically restrained the mice by pressing them down by hand for approximately 10 seconds. In the tail hanging experiments, the mice were suspended upside down by their tail for 10 seconds. In the ARS assay, photometry signals were recorded through the fiber coupled cannulae that passed through a modified ARS-inducing falcon tube to allow unrestricted recording. On the hot-plate test the mice were acclimitized to the equipment with the optic fiber connected to the cannulae a day before experimentations. During the experiments, the equipment was first allowed to reach the desired temperature and then the animals were introduced on the hot-plate test.

Immunostaining, multiplex in situ hybridization, and confocal microscopy

Mice were anesthetized with isoflurane and perfused intracardially with 1X PBS (Takara) and 4% PFA (Ted Pella, Inc.), consecutively for immunostaining experiments. Fresh brains were harvested for in situ hybridization experiments. For the cFos experiments, brains were harvested 90 mins after ARS assay, and 150 mins after i.p. CNO administration. Tissue sections were rinsed in 1X PBS, and incubated in a blocking buffer (2% Bovine Serum Albumin; 0.3% Triton X-100; PBS) for 1 hour at room temperature. Sections were incubated in primary

antibodies in blocking buffer at room temperature overnight. Sections were rinsed 1-2 times with PBS, and incubated for 2 hours in Alexa Fluor conjugated goat anti-rabbit/ chicken or donkey anti-goat/rabbit secondary antibodies (Invitrogen) at room temperature, washed in PBS, and mounted in VectaMount permanent mounting media (Vector Laboratories Inc.) onto charged glass slides (Globe Scientific Inc.). Multiplex ISH was done with a manual RNAscope assay (Advanced Cell Diagnostics). Probes were ordered from the ACD online catalog. We used a upright fluorescence microscope (Khush, Bengaluru) (2.5X, 4X, and 10X lens) and ImageJ/FIJI image processing software to image, and process images for the verification of anatomical location of cannulae implants. For the anatomical studies the images were collected with10X and 20X objective on a laser scanning confocal system (Leica SP8 Falcon), and processed using the Leica image analysis suite. For the Airy Scan Imaging, Zeiss 980 was used (NCBS Central Imaging Core facility).

CUBIC clearing and imaging

In order to visualize the fluorescent neuronal labeling in the cleared brain tissue, 300um thick sections were cleared by first washing with 1X PBS for 30 minutes, followed by 2-hour incubation in 50% Cubic L solution [94]. Next, the sections were immersed and incubated in 100% Cubic L solution overnight at 37°C. The sections were preserved and imaged in the Cubic R+ solution. For imaging the cleared sections, 10X and 20X objectives were used along with the Leica SP8 Confocal microscope.

CNO Encapsulation

CNO was encapsulated within poly-lactic-*co*-glycolic acid (PLGA, M_w 10–15 kDa, LG 50:50, PolySciTech, IN, USA) microparticles using a single emulsion method. Briefly, 100 mg PLGA and 2 mg CNO were dissolved in 1 ml dichloromethane (DCM) and mixed for 10 minutes. This mixture was homogenized (IKA® T18 digital Ultra Turrax) with 10 ml 1% polyvinyl alcohol (PVA) at 12000 rpm, resulting in an emulsion. This emulsion was added to 100 ml 1% PVA with magnetic stirring to allow DCM to evaporate. After 4 hours, the microparticles were collected by centrifugation (8000 *g*) and washed thrice with deionized water to remove PVA. The suspension was frozen, followed by lyophilization to obtain the CNO-encapsulated microparticles as powder. For experiments, the powder was weighed and resuspended in 1X PBS to get a concentration of 0.5 mg/mL.

Quantification and Statistical Analysis

All statistical analyses were performed using GraphPad PRISM 8.0.2 software. ns > 0.05, * $p \leq 0.05$, ** $p \leq 0.01$, *** $p \leq 0.001$, **** $p \leq 0.0005$.

Figure legends

Figure1. LS neurons are engaged by acute stress due to physical restraint. (A) Schematic representing the Acute Restraint Stress (ARS) assay used to induce stress in mice. (B) Location of the Lateral Septum (LS) — medial to the caudate putamen (CP) and inferior to the rostrum of the Corpus Callosum (CC) (AP: +0.50, ML: +0.25, DV: -2.50). (C) cFos expression in the LS of restrained mice compared to unrestrained control mice (Green-cFos, Red-neurotrace). (D) Multiplex Insitu hybridization with VGlut2 and VGat (red-VGat, green-VGlut2). (E) AAVs encoding Gad67-Cre and DIO-GCaMP6s were co-injected in the LS, and fiber optic cannulaes were implanted above for recording neural activity. (F) Confirmation of the expression of GCaMP6s (Green) in the LS neurons. (G) Schematic representation of the fiber photometry system (left). Neural activity recorded from control GFP (green) and GCaMP6s (blue) mice freely moving in their homecage (right). (H) Neural activity from the LS while mice were under restraint. (I) Traces of neural activity when mice were allowed to move freely in the homecage (blue), and when they were under restraint (red). Peaks corresponding to neural activity (blue dashes) were seen when mice struggled in the tube. (J) Heatmap depicting neural activity during individual instances of struggles. (K and L) Average plot and heatmap (individual trials) of Z-Score traces (5 mice) during immobilization. (M and N) Average plot and heatmap (individual trials) of Z-Score traces (5 mice) during tail suspension. (O, P, S and T) Average plots and heatmaps for LS responses on the hot-plate at 32 deg before and after intraplantar (i.pl.) CFA injection. (Q, R, U and V) Average plots and heatmaps for LS engagement on the hot plate at a noxious temperature of 52 deg before and after i.pl. CFA injection.

Figure2. Transient activation of LS neurons suppresses responses to noxious thermal stimuli. (A) Gad67-Cre and DIO-tdTomato were injected in the LS of wild-type mice. (B) tdTomato-positive cells (red) and cFos expression (green) post-saline or DCZ administration (i.p.). (C) Tail-flick latency in $LS^{Gad67\text{-}tdTomato}$ mice post i.p. Saline or DCZ administration. (D) Licks, latency to lick, shakes and latency to shake on the hot-plate test of $LS^{Gad67\text{-}tdTomato}$ mice, administered with either i.p. Saline or DCZ. Same parameters were measured in mice with i.pl. CFA to cause persistent inflammatory pain. (E) AAVs encoding Gad67-Cre and DIO-hM3Dq-mCherry were stereotaxically injected in the LS of wild-type mice to express the excitatory DREADD. (F) i.p. Saline or DCZ evoked cFos expression (green) in the mCherry-positive cells (red) in the $LS^{Gad67\text{-}hM3Dq}$ neurons. (G) Tail-flick latency (t-test, $^{**}P$=0.01, n=7) post-saline or DCZ administration in $LS^{Gad67\text{-}hM3Dq}$ mice . (H) Licks (t-test, $^{*}P$=0.05, n=7), shakes, latency to lick (t-test, $^{*}P$=0.05, n=7), shakes and latency to shake on the hot-plate test of $LS^{Gad67\text{-}tdTomato}$ mice, administered with either i.p. Saline or DCZ. Same parameters were measured post i.pl. CFA; licks (t-test, $^{*}P$=0.05, n=7), latency to lick (t-test, $^{*}P$=0.05, n=7). (I) Gad67-Cre and DIO-GFP were injected in the LS of wild-type mice. (J) cFos expression (red) with (ON) and without (OFF) blue light illumination in the $LS^{Gad67\text{-}GFP}$ neurons (green). (K) Tail-flick latency in $LS^{Gad67\text{-}GFP}$ with (ON) and without (OFF) blue light illumination. (L) Licks, latency to lick, shakes and latency to shake on the hot-plate test of $LS^{Gad67\text{-}GFP}$ mice before and after i.pl. CFA injection. (M) Gad67-Cre and DIO-ChR2-YFP were injected in the LS of wild-type mice to label the LS inhibitory neurons with excitatory opsin. (N) cFos (red) expression seen in the YFP-positive cells (green) upon blue light illumination. (O) Tail-flick latency (t-test, $^{***}P$= 0.001, n=7) with (ON) and without

(OFF) blue light illumination. (P) Licks (t-test, ***P=0.001, n=7), latency to lick (t-test, ***P= 0.001, n=7), shakes and latency to shake on the hot-plate test of $LS^{Gad67\text{-}tdTomato}$ mice, administered with either i.p. Saline or DCZ. Same parameters were measured in mice with i.pl. CFA; licks (t-test, ***P=0.001, n=7), latency to lick (t-test, ***P= 0.001, n=7).

Supplementary Figure1. (A, B) Rostrocaudal distribution of cFos in the LS of wild-type mice in the response to ARS. (C) Blood corticosterone levels in mice administered with saline, DCZ, or subjected to ARS. (D) Sample traces demonstrating time spent by $LS^{Gad67\text{-}hM3Dq}$ mice in the lit chamber of the classic light-dark box assay to test stress-induced anxiety. (E) Time spent in the light box post-saline or DCZ administration (t-test, **P=0.01, n=6). (F, G, H, I) Number of licks (t-test, **P=0.01, n=5), temperature of lick onset (t-test, ***P=0.001, n=5), number of shakes, and temperature of shake onset (t-test, ***P=0.001, n=5) post i.pl. CFA injection on a 32-56 degree gradient on the hot plate. (J and K) Number and latency of jumps post saline or DCZ administration on the hot plate before and after i.pl. CFA injection in $LS^{Gad67\text{-}hM3Dq}$ mice. (L and M) Number and latency of jumps post-DCZ administration before and after i.pl. CFA injection in $LS^{Gad67\text{-}tdTomato}$ mice.

Figure 3. LS neurons are required for acute stress-induced pain suppression. (A) Gad67-Cre and DIO-GFP were co-injected in the LS of wild-type mice. (B) GFP-positive neurons (green) seen in the LS. (C) Tail-flick latency (t-test, ***P=0.001, n=8) with and without restraint for 1 hour using the ARS assay in $LS^{Gad67\text{-}GFP}$mice. (D) Number of licks (t-test, **P=0.01, n=7), latency to lick (t-test, ***P=0.001, n=7), shakes and latency to shake with and without restraint in in $LS^{Gad67\text{-}GFP}$mice. Same parameters were measured post i.pl. CFA injection, licks (t-test, **P=0.01, n=7), latency to lick (t-test, *P=0.05, n=7). (E) Gad67-Cre and DIO-Tettox-GFP were injected in the LS of wild-type mice to allow TetTox expression inhibitory neurons. (F) GFP-positive cells (green) seen in the LS. (G) Tail-flick latency with and without restraint in $LS^{Gad67\text{-}GFP}$mice. (H) Number and latency of licks and shakes with and without restraint before and after i.pl. CFA injection in $LS^{Gad67\text{-}GFP}$mice. (I) Gad67-Cre and DIO-GFP were injected in the LS of wild-type mice. (J) GFP-positive cells (green) seen in the LS. (K) Tail-flick latency of mice subjected to ARS with (ON) (t-test, ***P=0.001, n=7) and without (OFF) (t-test, ***P=0.001, n=7) yellow light illumination. (L) Number of licks (t-test, **P=0.01, n=7), latency to lick (t-test, ***P=0.001, n=7), shake, and latency to shake in mice subjected to ARS with yellow light (ON and OFF). (M) Gad67-Cre and DIO-eNpHR3.0-YFP were co-injected in the LS of wild-type mice. (N) YFP-positive cells (green) in the LS to confirm eNpHR3.0 expression. (O) Tail-flick latency in $LS^{Gad67\text{-}eNpHR3.0}$ mice under restraint, with light ON (t-test, ***P=0.001, n=7; compared to light OFF) and (t-test, **P=0.01, n=7, compared unrestrained OFF). (P) Number of licks in $LS^{Gad67\text{-}eNpHR3.0}$ mice under restraint, with light ON (t-test, **P=0.01, n=7; compared with light OFF) and (t-test, ***P=0.001, n=7, compared unrestrained OFF); lick latency (t-test, **P=0.01, n=7; compared with light OFF) and (t-test, **P=0.01, n=7, compared unrestrained OFF); shakes and shake latency.

Supplementary Figure2. (A) AAVs encoding Gad67-Cre, DIO-hM3Dq-mCherry, and DIO-TetTox-GFP or DIO-GFP injected in the LS of wild-type mice to simultaneously label the LS^{Gad67} neurons with the excitatory DREADD, and TetTox. Overlapping yellow cells representing

hM3Dq (red), and TetTox (green) co-expressing neurons in the LS. (B) Tail-flick latency in $LS^{Gad67\text{-}TetToxGFP\text{-}hM3Dq}$ mice (t-test, ***P*=0.01, n=4), and in $LS^{Gad67\text{-}TetTox\text{-}hM3Dq}$ mice post saline or DCZ administration (C) Tail-flick latencies of mice with and without restraint at different time points post the ARS assay (Immediate t-test, **P*=0.05, n=4) (Post-10 mins t-test, ***P*=0.01, n=4) (Post 30 mins t-test, ***P*=0.01, n=4). (D) Tail-flick latencies over an hour of $LS^{Gad67\text{-}ChR2}$ mice post blue light illumination for 30 minutes (t-test, **P*=0.05, n=4) (Post-10 mins t-test, ***P*=0.01, n=4) (Post 30 mins t-test, ***P*=0.01, n=4). (E) Gad67-cre and DIO-GFP injected in the LS of wild-type mice. (F) Number and latency of jumps with and without restraint before and after i.pl. CFA injection. (G) Gad67-cre and DIO-Tettox-GFP injected in the LS of wild-type mice. (H) Number and latency of jumps with and without restraint before and after i.pl. CFA injection. (I) Number of licks in $LS^{Gad67\text{-}eNpHR3.0}$ mice under restraint post i.pl. CFA injection, with light ON (t-test, ****P*= 0.001, n=7; compared with light OFF) and (t-test, ****P*=0.001, n=7, compared unrestrained OFF); lick latency (t-test, ****P*=0.001, n=7; compared with light OFF) and (t-test, ****P*=0.001, n=7, compared unrestrained OFF); shakes, and shake latency. (J) Number of licks, latency to lick, shakes and latency to shake in $LS^{Gad67\text{-}GFP}$ mice under restraint post i.pl. CFA injection, with (ON) and without (OFF) yellow light illumination.

Figure4. LS neurons synapse onto an excitatory subpopopulation of LH neurons. (A) Gad67-Cre and DIO-GFP injected in the LS of wild-type mice. (B) GFP-positive cells seen in the LS. Green projections from the LS were seen in the Habenula (Hb) and Lateral Hypothalamus (LH). (C) Gad67-Cre and DIO-SynRuby injected in the LS of wild-type mice. (D) Ruby expression was seen at the injection site and post-synaptic region (LH). (E) AAV1-FlpO injected in the LS; fDIO-tdTomato, and DIO-GFP injected in the LH of VGlut2-Cre transgenic mice. (F) Overlapping red and green cells (yellow) were seen in the LH. (G) AAVTransyn-Cre injected in the LS of Ai14 transgenic mice. (H) The LH was labeled with probes against VGlut2 using in situ hybridization. Co-localisation of tdTomato-positive (red) and GFP-positive (green) cells in the LH. (I) Gad67-Cre and DIO-Synaptophysin-GFP injected in the LS and DIO Gephyrn-tagRFP in the LH of VGlut2-Cre transgenic mice. (J) Closely apposed green synaptophysin and red gephyrin puncta seen in the LH. (K) AAVTransyn-Cre injected in the LS and DIO-GCaMP6s in the LH of wild-type mice to record neural activity from the $LH_{post\text{-}LS}$ neurons. (L) GFP-positive cells (green) and tissue injury from the fiber implant seen in the LH. (M) Left to right: Heat maps depicting neural activity in $LH_{post\text{-}LS}$ neurons during the entire struggle duration, first three seconds of the struggle, and last ten seconds of the struggle in the ARS assay tube, respectively. (N) Left to right: Heat maps depicting neural activity in LS^{Gad67} neurons during the entire struggle duration, first three seconds of the struggle, and last ten seconds of the struggle in the ARS assay tube, respectively.

Supplementary Figure 3. (A) Rostral to caudal serial images of the LH taken on a fluorescence microscope at 4X and 10X magnifications showing projections from the LS, post Gad67-Cre and DIO-GFP injections in the LS of wild-type mice. (B) Allen Brain Atlas images showing the anatomical location of the LH next to the parasubthalamic nucleus (PSTN). (C) In situ hybridization using probes against VGlut2 and VGat performed on LH sections of wild-type mice (red: vglut2, green: vgat). (D) Parvalbumin staining in the LH sections. (E and F) Average plot and heatmap of 20 individual Z-Score traces across 5 mice of neural activity from $LH_{post\text{-}LS}$

neurons during immobilization trials. (G and H) Average plot and heatmap of 20 individual Z-Score traces across 5 mice of neural activity from $LH_{post\text{-}LS}$ neurons during tail suspension trials. (I and J) Average plot and heatmap of $LH_{post\text{-}LS}$ neurons on the hot plate at an innocuous temperature of 32 deg. (K and L) Average plot and heatmap of $LH_{post\text{-}LS}$ neurons on the hot plate at a noxious temperature of 52 deg.

Figure5. LS→LH circuitry is sufficient and necessary for ARS-induced analgesia. (A) Gad67-Cre and DIO-ChR2-YFP injected in the LS of wild-type mice to express the excitatory opsin ChR2 in the LS^{Gad67} neurons. The fiber was implanted in the LH to facilitate terminal activation. ChR2-YFP-positive terminals observed in the LH. (B) Tail-flick latency (t-test, ***P=0.001, n=7) with (ON) and without (OFF) blue light illumination in $LS^{Gad67\text{-}GFP}$ mice (C) Licks (t-test, ***P=0.001, n=7), latency to lick (t-test, ***P=0.001, n=7), shakes and latency to shake on the hot plate with (ON) and without (OFF) blue light illumination in $LS^{Gad67\text{-}GFP}$ mice. Same parameters were measured post i.pl. CFA injection; licks (t-test, ***P=0.001, n=7), latency to lick (t-test, ***P=0.001, n=7). (D) AAVRetro-Cre injected in the LH and DIO-tdTomato in the LS of wild-type mice. Presence of tdTomato-positive cells (red) in the LS. (E) Tail-flick latency in $LS_{pre\text{-}LH}{}^{Gad67\text{-}tdTomato}$ mice post saline or DCZ administration. (F) Number and latency of licks and shakes post saline or DCZ administration in $LS_{pre\text{-}LH}{}^{Gad67\text{-}tdTomato}$ mice before and after i.pl. CFA injection. (G) AAVRetro-Cre injected in the LH and DIO-hM3Dq-mCherry in the LS of wild-type mice to express the excitatory DREADD. Presence of mCherry-positive cells (red) co-localised with cFos-positive cells (green) in the LS. (H) Tail-flick latency (t-test, ***P=0.001, n=7) post saline or DCZ administration in $LS_{pre\text{-}LH}{}^{Gad67\text{-}hM3Dq}$ mice. (I) Number of licks (t-test, *P=0.05, n=7), latency to lick (t-test, *P=0.05, n=7), shakes and latency to shake post saline or DCZ administration in $LS_{pre\text{-}LH}{}^{Gad67\text{-}hM3Dq}$ mice. Same parameters were measured post i.pl. CFA injection; licks (t-test, **P=0.01, n=7), latency to lick (t-test, *P=0.05, n=7). (J) AAVTransyn-Cre injected in the LS and DIO-tdTomato in the LH of wild-type mice. Presence of tdTomato-positive cells (red) in the LH. (K) Tail-flick latency post saline or DCZ administration in $LH_{post\text{-}LS}{}^{hM3Dq}$ mice. (L) Number and latency of licks and shakes post saline or DCZ administration $LH_{post\text{-}LS}{}^{tdTomato}$ mice before and after i.pl. CFA injection. (M) AAVTransyn-Cre injected in the LS and DIO-hM3Dq-mCherry in the LH of wild-type mice to express the excitatory DREADD. Presence of mCherry-positive cells (red) co-localised with cFos-positive cells (green) in the LH. (N) Tail-flick latency (t-test, ***P=0.001, n=7) post saline or DCZ administration in $LH_{post\text{-}LS}{}^{hM3Dq}$ mice. (O) Number of licks (t-test, *P=0.05, n=7), latency to lick (t-test, **P=0.01, n=7), shakes and latency to shake post saline or DCZ administration $LH_{post\text{-}LS}{}^{tdTomato}$ mice. Same parameters were measured post i.pl. CFA injection; licks (t-test, *P= 0.05, n=7), latency to lick (t-test, *P=0.05, n=7). (P) AAVTransyn-Cre injected in the LS and DIO-hM3Dq-mCherry in the Habenula (Hb) of wild-type mice to express the excitatory DREADD. Presence of mCherry-positive cells (red) in the Hb. (Q) Tail-flick latency post saline or DCZ administration in $Hb_{post\text{-}LS}{}^{hM3Dq}$ mice. (R) Number and latency of licks and shakes post saline or DCZ administration in $Hb_{post\text{-}LS}{}^{hM3Dq}$ mice. (S) AAVTransyn-Cre injected in the LS and DIO-GFP bilaterally in the LH of wild-type mice . Presence of GFP-positive cells (green) in the LH. (T) Tail-flick latency (t-test, ***P=0.001, n=7) with and without restraint in $LH_{post\text{-}LS}{}^{GFP}$ mice. (U) Number of licks (t-test, ***P=0.001, n=7), latency to lick (t-test, **P=0.001, n=7), shakes and latency to shake with and without restraint in $LH_{post\text{-}LS}{}^{GFP}$ mice. Same parameters were measured post i.pl. CFA injection; licks (t-test, ***P=0.001, n=7), latency

to lick (t-test, ***P=0.001, n=7). (V) AAVTransyn-Cre injected in the LS and DIO-Tettox-GFP bilaterally in the LH of wild-type mice. Presence of GFP-positive cells (green) in the LH. (W) Tail-flick latency with and without restraint in $LH_{post\text{-}LS}^{TetTox}$ mice. (X) Number and latency of licks and shakes with and without restraint in $LH_{post\text{-}LS}^{TetTox}$ mice.

Supplementary Figure4. (A) Absorption spectra for the vehicle DMSO (green) and CNO dissolved in DMSO (red). (B) Cy3 fluorescent beads as seen under the microscope at 100X with oil immersion. (C) Cy3 fluorescent beads injected in the LS and images under the fluorescence microscope at 4X and 10X magnifications. (D) Gad67-Cre and DIO-tdTomato injected in the LS of wild-type mice. 3 weeks later, CNO beads were injected stereotaxically in the LS over the same co-ordinates. (E) Tail-flick latency over the course of 8 days post-CNO beads injection in $LS^{Gad67\text{-}hM3Dq}$ mice. (F) Number and latency of licks and shakes post-CNO beads injection in $LS^{Gad67\text{-}hM3Dq}$ mice. (G) Gad67-Cre and DIO-hM3Dq-mCherry stereotaxically injected in the LS of wild-type mice to express the excitatory DREADD. 3 weeks later, CNO beads were injected stereotaxically in the LS over the same co-ordinates. (H) Tail-flick latency (Day2 t-test, **P= 0.01, n=7) (Day4 t-test, ***P=0.001, n=7) over a course of 8 days post CNO beads injection. (I) Number of licks (Day2 t-test, **P=0.01, n=7) (Day4 t-test, **P=0.01, n=7), latency to lick (Day2 t-test, *P=0.05, n=7) (Day4 t-test, *P=0.05, n=7), shakes (Day2 t-test, **P=0.01, n=7) (Day4 t-test, ***P=0.001, n=7), and latency to shake over a course of 8 days post CNO beads injection. (J) Gad67-Cre and DIO-hM3Dq injected in the LS of wild-type mice. 3 weeks later, CNO beads were injected in the LH to enable terminal activation of $LH_{post\text{-}LS}$ neurons. (K) Tail-flick latency (Day2 t-test, ***P=0.001, n=7) (Day4 t-test, ***P=0.001, n=7) over a course of 8 days post CNO beads injection. (L) Number of licks (Day2 t-test, *P=0.05, n=7) (Day4 t-test, *P =0.05, n=7), latency to lick (Day2 t-test, *P=0.05, n=7) (Day4 t-test, **P=0.01, n=7), shakes and latency to shake over a course of 8 days post CNO beads injection.

Figure 6. RVM ON-cells are downstream of the LS→LH circuitry. (A) AAVTransyn-Cre injected in the LS and DIO-GFP in the LH of wild-type mice to label the $LH_{post\text{-}LS}$ neurons. (B) GFP-positive cell bodies in the LH (green, left). Projections of the $LH_{post\text{-}LS}$ neurons in the PBN, and RVM. (C) Presence of fluorescence (black) in RVM post tissue clearing of the same brains expressing GFP in the $LH_{post\text{-}LS}$ neurons. (D) AAVTransyn-Cre injected in the LH and DIO-GFP in the RVM of wild-type mice to label the $RVM_{post\text{-}LH}$ neurons with GFP. (E) GFP-positive cell bodies (black) seen in the RVM. (F) Projections from the $RVM_{post\text{-}LH}$ were observed in the lumbar spinal cord. (G) AAVTransyn-Cre injected in the LS, and DIO-G and DIO-TVA-GFP in the LH of wild-type mice. Three weeks later, the delG-Rabies-mCherry virus was injected into the RVM. (H) Starter cells (yellow) observed in the LH. mCherry-positive cell bodies (red) seen in the LS. (I) AAVRetro-FlpO injected in the RVM, fDIO-Post-GRASP injected in the LH, and Pre-GRASP in the LS of wild-type mice. (J) Axon terminals from the LS neurons (Green) were observed around the $LH_{pre\text{-}RVM}$ (red) cell-bodies. (K) AAVTransyn-Cre was injected in the LH with DIO-GCaMP6s in the RVM of wild-type mice. A fiber was implanted on the RVM over the same co-ordinates to perform fiber-photometry. (L) GFP-positive cells in the RVM (green) to demonstrate successful expression of GCaMP6s in the $RVM_{post\text{-}LH}$ neurons. (M) Z-Score of calcium dynamivs recorded from the $RVM_{post\text{-}LH}$ neurons while the mice are restrained and struggling (blue dashes) in a falcon tube. (N) The average plot of 20 individual struggle traces from 4 mice. (O)

(Left to right) Heatmaps depicting neural activity patterns during individual instances of struggle in the falcon tube, licks, and shakes on the hot plate at 52 degrees, respectively.

Supplementary Figure 5. (A) AAVTransyn-Cre injected in the LH, and DIO-SynRuby injected in the RVM of wild-type mice. (B) Red cell bodies expressing SynRuby were observed in the RVM. (C) Red puncta of $RVM_{post\text{-}LH}$ axon terminals observed in the LH. (D) Axon terminals of the $RVM_{post\text{-}LH}$ neurons seen in the dorsal horn of the lumbar spinal cord (E) DIO-SynGFP injected in the LH, and DIO-PSD95-tagRFP in the RVM of VGlut2-Cre transgenic mice. (F) Confocal images of the LH^{VGlut2} terminals (green), and RVM^{VGlut2} dendrites (red) observed under 10X magnification. (G) Confocal images under 20X magnification of the same regions. (H) 40X Airyscan super-resolution image demsontrating close apposition between the red, and green puncta. (I) Gad67-Cre and DIO-hM3Dq injected in the LS of wild-type mice to express the excitatory DREADD, hM3Dq in the LS^{Gad67} neurons. (J) Number and latency of licks and shakes post-saline or DCZ administration in $LS^{Gad67\text{-}hM3Dq}$ mice i.p. injected with the mu-opioid receptor antagonist naltrexone.

Figure 7. Activation of $RVM_{post\text{-}LH}$ neurons results in thermal hyperalgesia, while inhibition was anti-nociceptive. (A) AAVTransyn-Cre injected in the LH and DIO-tdTomato in the RVM of wild-type mice. (B) mCherry-positive cells (red) in the RVM. (C) Tail-flick latency after i.p. saline or DCZ administration in $RVM_{post\text{-}LH}^{tdTomato}$ mice. (D) Number and latency of licks and shakes post saline or DCZ administration before and after i.pl. CFA injection in $RVM_{post\text{-}LH}^{tdTomato}$ mice. (E) AAVTransyn-Cre injected in the LH and DIO-hM3Dq in the RVM of wild-type mice to express the excitatory DREADD in the $RVM_{post\text{-}LH}$ neurons. (F) DCZ induced c-Fos (green) expression in the $RVM_{post\text{-}LH\text{-}hM3Dq}$ (red, arrow heads) neurons. (G) Tail-flick latency (t-test, ***P=0.001, n=7) post saline or DCZ administration in the $RVM_{post\text{-}LH\text{-}hM3Dq}$ mice. (H) Number of licks (t-test, **P=0.01, n=7), latency to lick (t-test, *P=0.05, n=7), shakes (t-test, *P=0.05, n=7), and latency to shake (t-test, *P=0.05, n=7) post saline or DCZ administration in the $RVM_{post\text{-}LH\text{-}hM3Dq}$ mice. Same parameters were measured post i.pl. CFA injection; licks (t-test, **P=0.01, n=7), latency to lick (t-test, **P=0.01, n=7), shakes (t-test, **P=0.01, n=7), latency to shake (t-test, *P=0.05, n=7). (I) AAVTransyn-Cre injected in the LH and DIO-hM4Di in the RVM of wild-type mice to express the inhibitory DREADD in the $RVM_{post\text{-}LH}$ neurons. (J) hM3Dq-mCherry expressing neurons (red) in the RVM. (K) Tail-flick latency (t-test, **P=0.01, n=7) post saline or DCZ administration in $RVM_{post\text{-}LH\text{-}hM4Di}$ mice. (L) Number of licks (t-test, ***P= 0.001, n=7), latency to lick (t-test, **P=0.01, n=7), shakes and latency to shake post saline or DCZ administration in $RVM_{post\text{-}LH\text{-}hM4Di}$ mice. Same parameters were measured post i.pl. CFA injection; licks (t-test, **P=0.01, n=7), latency to lick (t-test, *P=0.05, n=7). (M) AAVTransyn-Cre injected in the LH and DIO-hM4Di in the PBN (bilaterally) of wild-type mice to express the inhibitory DREADD, hM4Di in the $lPBN_{post\text{-}LH}$ neurons. (N) hM4Di-mCherry (red) expressing neurons in the PBN. (O) Tail-flick latency post-saline or DCZ administration in the $PBN_{post\text{-}LH\text{-}hM4Di}$ mice. (P) Number and latency of licks and shakes post-saline or DCZ administration before and after i.pl. CFA injection in the $PBN_{post\text{-}LH\text{-}hM4Di}$ mice. (Q) AAVTransyn-Cre injected in the LH and DIO-GFP in the RVM of wild-type mice to label the $RVM_{post\text{-}LH}$ neurons. Optic fiber cannulae was implanted over the RVM at same coordinates to deliver blue light. (R) GFP-positive cells (green) observed in the $RVM_{post\text{-}LH}$ neurons. (S) Tail-flick latency with (ON) and without (OFF) yellow

light illumination in $RVM_{post\text{-}LH}^{GFP}$ mice. (T) Number and latency of licks and shakes with (ON) and without (OFF) yellow light illumination before and after i.pl. CFA injection in $RVM_{post\text{-}LH\text{-}GFP}$ mice. (U) AAV-transsynaptic-Cre injected in the LH and DIO-eNPHR3.0-YFP in the RVM of wild-type mice to express the inhibitory opsin. An optic fiber was implanted in the RVM over the same coordinates. (V) YFP-positive cells expressing eNpHR3.0 in the $RVM_{post\text{-}LH}$ (green) neurons in the RVM. (W) Tailflick latency (t-test, ***P=0.001, n=7) with (ON) and without (OFF) yellow light illumination. (X) Number of licks (t-test, ***P=0.001, n=7), latency to lick (t-test, ***P=0.001, n=7), shakes and latency to shake with (ON) and without (OFF) yellow light illumination in $RVM_{post\text{-}LH}^{eNPHR3.0}$ mice. Same parameters were measured post i.pl. CFA injection; licks (t-test, **P=0.01, n=7), latency to lick (t-test, ***P=0.001, n=7).

Figure 8. lPAG neurons project to the LS and communicates escape responses in mice under restraint. (A) AAVRetro-nls-mCherry injected in the LS of wild-type mice. (B) mCherry expressing cells (red) in the LS and nuclei projecting to the LS (LH, and the lateral periaqueductal gray (lPAG). (C) AAVTransyn-Cre injected in the lPAG; DIO-GFP and tagRFP in the LS of wild-type mice. (D) Presence of tagRFP (red) and GFP (green) expressing LS axon terminals in the LH. (E) AAVRetro-Cre injected in the LH, and DIO-G, DIO-TVA-GFP, and delG-Rabies-mCherry in the LS of wild-type mice. (F) Starter cells (yellow) in the LS. mCherry-positive cells (red) were observed in the Hippocampus, the LH, and the lPAG. (G) AAVTransyn-Cre injected in the lPAG and DIO-hM3Dq in the LS of wild-type mice to express the excitatory DREADD. (H, I, J, K) Number of licks (t-test, **P=0.01, n=7), temperature of lick onset (t-test, *P=0.05, n=7), shakes (t-test, *P=0.05, n=7), and temperature of shake onset (t-test, **P=0.01, n=7) on the hot plate at a gradient from 32-56 degrees post-saline or DCZ administration (i.p.) in the $LS_{post\text{-}lPAG}^{hM3Dq}$ mice. Same parameters were measured post-i.pl. CFA injection; licks (t-test, ***P=0.001, n=7), temperature of lick onset (t-test, **P=0.01, n=7), shakes (t-test, ***P=0.001, n=7), and temperature of shake onset (t-test, ***P=0.001, n=7). (L) DIO-GCaMP6s injected in the lPAG of VGlut2-Cre transgenic mice. GCaMP6s (green) expressing cells and in the lPAG. (M) Heatmap showing neural recordings from the lPAG neurons during ARS. (N) Bar graph depicting the AUC of the photometry recordings during the struggle bouts from the PAG, LS^{Gad67}, $LH_{post\text{-}LS}$, and $RVM_{post\text{-}LH}$ neurons.

Supplementary Figure 6. (A) Axon terminals of the LS neurons in the LH labeled by AAVTrans-Cre injected in the lPAG; DIO-GFP and tagRFP in the LS of wild-type mice. (B) Rostral to caudal distribution of LS neurons in the LH (C) DIO-Synaptophysin-GFP injected in the lPAG; Gad67-Cre and DIO-PSD95-RFP in the LS of VGlut2-Cre transgenic mice. (D, E) Close apposition of the red (PSD95-RFP) and green (Synaptophysin-GFP) puncta observed under the confocal microscope at 20X (D), and 40X (E) magnification. (F) Diagramatic representation of the LS-centric ARS-induced SIA pathway that originates from lPAG and terminates in the spinal cord via LH and RVM.

References

1. Tracey, I., and Mantyh, P.W. (2007). The cerebral signature for pain perception and its modulation. Neuron *55*, 377–391.

2. Gol, A. (1967). Relief of pain by electrical stimulation of the septal area. Journal of the Neurological Sciences *5*, 115–120. 10.1016/0022-510x(67)90012-3.

3. Olds, J., and Milner, P. (1954). Positive reinforcement produced by electrical stimulation of septal area and other regions of rat brain. J. Comp. Physiol. Psychol. *47*, 419–427.

4. Abbott, F.V., and Melzack, R. (1978). Analgesia produced by stimulation of limbic structures and its relation to epileptiform after-discharges. Exp. Neurol. *62*, 720–734.

5. Köhler, C. (1976). Habituation of the orienting response after medial and lateral septal lesions in the albino rat. Behav. Biol. *16*, 63–72.

6. Albert, D.J., and Wong, R.C. (1978). Hyperreactivity, muricide, and intraspecific aggression in the rat produced by infusion of local anesthetic into the lateral septum or surroundng areas. Journal of Comparative and Physiological Psychology *92*, 1062–1073. 10.1037/h0077524.

7. Brady, J.V., and Nauta, W.J. (1953). Subcortical mechanisms in emotional behavior: affective changes following septal forebrain lesions in the albino rat. J. Comp. Physiol. Psychol. *46*, 339–346.

8. Brady, J.V., and Nauta, W.J. (1955). Subcortical mechanisms in emotional behavior: the duration of affective changes following septal and habenular lesions in the albino rat. J. Comp. Physiol. Psychol. *48*, 412–420.

9. Rizzi-Wise, C.A., and Wang, D.V. (2021). Putting Together Pieces of the Lateral Septum: Multifaceted Functions and Its Neural Pathways. eNeuro *8*. 10.1523/ENEURO.0315-21.2021.

10. Anthony, T.E., Dee, N., Bernard, A., Lerchner, W., Heintz, N., and Anderson, D.J. (2014). Control of stress-induced persistent anxiety by an extra-amygdala septohypothalamic circuit. Cell *156*, 522–536.

11. Sheehan, T.P., Chambers, R.A., and Russell, D.S. (2004). Regulation of affect by the lateral septum: implications for neuropsychiatry. Brain Res. Brain Res. Rev. *46*, 71–117.

12. Terrill, S.J., Maske, C.B., and Williams, D.L. (2018). Endogenous GLP-1 in lateral septum contributes to stress-induced hypophagia. Physiol. Behav. *192*, 17–22.

13. Singewald, G.M., Rjabokon, A., Singewald, N., and Ebner, K. (2011). The modulatory role of the lateral septum on neuroendocrine and behavioral stress responses. Neuropsychopharmacology *36*, 793–804.

14. Siemian, J.N., Arenivar, M.A., Sarsfield, S., Borja, C.B., Erbaugh, L.J., Eagle, A.L., Robison, A.J., Leinninger, G., and Aponte, Y. (2021). An excitatory lateral hypothalamic circuit orchestrating pain behaviors in mice. Elife *10*. 10.7554/eLife.66446.

15. Carr, K.D., and Uysal, S. (1985). Evidence of a supraspinal opioid analgesic mechanism

engaged by lateral hypothalamic electrical stimulation. Brain Res. *335*, 55–62.

16. Holden, J.E., and Pizzi, J.A. (2008). Lateral hypothalamic-induced antinociception may be mediated by a substance P connection with the rostral ventromedial medulla. Brain Res. *1214*, 40–49.

17. Dafny, N., Dong, W.Q., Prieto-Gomez, C., Reyes-Vazquez, C., Stanford, J., and Qiao, J.T. (1996). Lateral hypothalamus: site involved in pain modulation. Neuroscience *70*, 449–460.

18. Franco, A.C., and Prado, W.A. (1996). Antinociceptive effects of stimulation of discrete sites in the rat hypothalamus: evidence for the participation of the lateral hypothalamus area in descending pain suppression mechanisms. Braz. J. Med. Biol. Res. *29*, 1531–1541.

19. Behbehani, M.M., Park, M.R., and Clement, M.E. (1988). Interactions between the lateral hypothalamus and the periaqueductal gray. J. Neurosci. *8*, 2780–2787.

20. Fuchs, P.N., and Melzack, R. (1995). Analgesia induced by morphine microinjection into the lateral hypothalamus of the rat. Exp. Neurol. *134*, 277–280.

21. Lefler, Y., Campagner, D., and Branco, T. (2020). The role of the periaqueductal gray in escape behavior. Curr. Opin. Neurobiol. *60*, 115–121.

22. Zimprich, A., Garrett, L., Deussing, J.M., Wotjak, C.T., Fuchs, H., Gailus-Durner, V., de Angelis, M.H., Wurst, W., and Hölter, S.M. (2014). A robust and reliable non-invasive test for stress responsivity in mice. Front. Behav. Neurosci. *8*, 125.

23. Bullitt, E. (1990). Expression of c-fos-like protein as a marker for neuronal activity following noxious stimulation in the rat. J. Comp. Neurol. *296*, 517–530.

24. Azevedo, E.P., Tan, B., Pomeranz, L.E., Ivan, V., Fetcho, R., Schneeberger, M., Doerig, K.R., Liston, C., Friedman, J.M., and Stern, S.A. (2020). A limbic circuit selectively links active escape to food suppression. Elife *9*. 10.7554/eLife.58894.

25. Kubo, T., Kanaya, T., Numakura, H., Okajima, H., Hagiwara, Y., and Fukumori, R. (2002). The lateral septal area is involved in mediation of immobilization stress-induced blood pressure increase in rats. Neurosci. Lett. *318*, 25–28.

26. Chen, T.-W., Wardill, T.J., Sun, Y., Pulver, S.R., Renninger, S.L., Baohan, A., Schreiter, E.R., Kerr, R.A., Orger, M.B., Jayaraman, V., et al. (2013). Ultrasensitive fluorescent proteins for imaging neuronal activity. Nature *499*, 295–300.

27. Gunaydin, L.A., Grosenick, L., Finkelstein, J.C., Kauvar, I.V., Fenno, L.E., Adhikari, A., Lammel, S., Mirzabekov, J.J., Airan, R.D., Zalocusky, K.A., et al. (2014). Natural neural projection dynamics underlying social behavior. Cell *157*, 1535–1551.

28. Porsolt, R.D. (2000). Animal models of depression: utility for transgenic research. Rev. Neurosci. *11*, 53–58.

29. Espejo, E.F., Stinus, L., Cador, M., and Mir, D. (1994). Effects of morphine and naloxone on behaviour in the hot plate test: an ethopharmacological study in the rat. Psychopharmacology *113*, 500–510.

30. Hylden, J.L.K., Nahin, R.L., Traub, R.J., and Dubner, R. (1989). Expansion of receptive

fields of spinal lamina I projection neurons in rats with unilateral adjuvant-induced inflammation: the contribution of dorsal horn mechanisms. Pain *37*, 229–243.

31. Dubner, R., Hylden, J.L.K., Nahin, R.L., and Traub, R.J. (1989). Neuronal Plasticity in the Superficial Dorsal Horn Following Peripheral Tissue Inflammation and Nerve Injury. Processing of Sensory Information in the Superficial Dorsal Horn of the Spinal Cord, 429–442. 10.1007/978-1-4613-0825-6_43.

32. Porro, C.A., and Carli, G. (1988). Immobilization and restraint effects on pain reactions in animals. Pain *32*, 289–307.

33. Armbruster, B.N., Li, X., Pausch, M.H., Herlitze, S., and Roth, B.L. (2007). Evolving the lock to fit the key to create a family of G protein-coupled receptors potently activated by an inert ligand. Proc. Natl. Acad. Sci. U. S. A. *104*, 5163–5168.

34. Krashes, M.J., Koda, S., Ye, C., Rogan, S.C., Adams, A.C., Cusher, D.S., Maratos-Flier, E., Roth, B.L., and Lowell, B.B. (2011). Rapid, reversible activation of AgRP neurons drives feeding behavior in mice. J. Clin. Invest. *121*, 1424–1428.

35. Nagai, Y., Miyakawa, N., Takuwa, H., Hori, Y., Oyama, K., Ji, B., Takahashi, M., Huang, X.-P., Slocum, S.T., DiBerto, J.F., et al. (2020). Deschloroclozapine, a potent and selective chemogenetic actuator enables rapid neuronal and behavioral modulations in mice and monkeys. Nat. Neurosci. *23*, 1157–1167.

36. Espejo, E. (1993). Structure of the rat's behaviour in the hot plate test. Behavioural Brain Research *56*, 171–176. 10.1016/0166-4328(93)90035-o.

37. Chapman, C.R., Casey, K.L., Dubner, R., Foley, K.M., Gracely, R.H., and Reading, A.E. (1985). Pain measurement: an overview. Pain *22*, 1–31.

38. Zhang, F., Wang, L.-P., Boyden, E.S., and Deisseroth, K. (2006). Channelrhodopsin-2 and optical control of excitable cells. Nat. Methods *3*, 785–792.

39. Rajendran, P.S., Challis, R.C., Fowlkes, C.C., Hanna, P., Tompkins, J.D., Jordan, M.C., Hiyari, S., Gabris-Weber, B.A., Greenbaum, A., Chan, K.Y., et al. (2019). Identification of peripheral neural circuits that regulate heart rate using optogenetic and viral vector strategies. Nat. Commun. *10*, 1944.

40. Carter, M.E., Han, S., and Palmiter, R.D. (2015). Parabrachial calcitonin gene-related peptide neurons mediate conditioned taste aversion. J. Neurosci. *35*, 4582–4586.

41. Kim, J.C., Cook, M.N., Carey, M.R., Shen, C., Regehr, W.G., and Dymecki, S.M. (2009). Linking genetically defined neurons to behavior through a broadly applicable silencing allele. Neuron *63*, 305–315.

42. Xu, W., Morishita, W., Buckmaster, P.S., Pang, Z.P., Malenka, R.C., and Südhof, T.C. (2012). Distinct neuronal coding schemes in memory revealed by selective erasure of fast synchronous synaptic transmission. Neuron *73*, 990–1001.

43. Xu, W., and Südhof, T.C. (2013). A neural circuit for memory specificity and generalization. Science *339*, 1290–1295.

44. Roper, J.A., Craighead, M., O'Carroll, A.-M., and Lolait, S.J. (2010). Attenuated stress

response to acute restraint and forced swimming stress in arginine vasopressin 1b receptor subtype (Avpr1b) receptor knockout mice and wild-type mice treated with a novel Avpr1b receptor antagonist. J. Neuroendocrinol. *22*, 1173–1180.

45. Gradinaru, V., Thompson, K.R., and Deisseroth, K. (2008). eNpHR: a Natronomonas halorhodopsin enhanced for optogenetic applications. Brain Cell Biol. *36*, 129–139.

46. Deng, K., Yang, L., Xie, J., Tang, H., Wu, G.-S., and Luo, H.-R. (2019). Whole-brain mapping of projection from mouse lateral septal nucleus. Biol. Open *8*. 10.1242/bio.043554.

47. Sweeney, P., and Yang, Y. (2016). An Inhibitory Septum to Lateral Hypothalamus Circuit That Suppresses Feeding. J. Neurosci. *36*, 11185–11195.

48. Shelton, L., Becerra, L., and Borsook, D. (2012). Unmasking the mysteries of the habenula in pain and analgesia. Prog. Neurobiol. *96*, 208–219.

49. Zingg, B., Peng, B., Huang, J., Tao, H.W., and Zhang, L.I. (2020). Synaptic Specificity and Application of Anterograde Transsynaptic AAV for Probing Neural Circuitry. J. Neurosci. *40*, 3250–3267.

50. Kitanishi, T., Tashiro, M., Kitanishi, N., and Mizuseki, K. (2022). Intersectional, anterograde transsynaptic targeting of neurons receiving monosynaptic inputs from two upstream regions. Commun Biol *5*, 149.

51. Zingg, B., Chou, X.-L., Zhang, Z.-G., Mesik, L., Liang, F., Tao, H.W., and Zhang, L.I. (2017). AAV-Mediated Anterograde Transsynaptic Tagging: Mapping Corticocollicular Input-Defined Neural Pathways for Defense Behaviors. Neuron *93*, 33–47.

52. Barik, A., Thompson, J.H., Seltzer, M., Ghitani, N., and Chesler, A.T. (2018). A Brainstem-Spinal Circuit Controlling Nocifensive Behavior. Neuron *100*, 1491–1503.e3.

53. Bensussen, S., Shankar, S., Ching, K.H., Zemel, D., Ta, T.L., Mount, R.A., Shroff, S.N., Gritton, H.J., Fabris, P., Vanbenschoten, H., et al. (2020). A Viral Toolbox of Genetically Encoded Fluorescent Synaptic Tags. iScience *23*, 101330.

54. Gross, G.G., Junge, J.A., Mora, R.J., Kwon, H.-B., Olson, C.A., Takahashi, T.T., Liman, E.R., Ellis-Davies, G.C.R., McGee, A.W., Sabatini, B.L., et al. (2013). Recombinant probes for visualizing endogenous synaptic proteins in living neurons. Neuron *78*, 971–985.

55. Jain, R.A. (2000). The manufacturing techniques of various drug loaded biodegradable poly(lactide-co-glycolide) (PLGA) devices. Biomaterials *21*, 2475–2490.

56. Sharma, P.R., Dravid, A.A., Kalapala, Y.C., Gupta, V.K., Jeyasankar, S., Goswami, A., and Agarwal, R. (2022). Cationic inhalable particles for enhanced drug delivery to M. tuberculosis infected macrophages. Biomaterials Advances *133*, 112612. 10.1016/j.msec.2021.112612.

57. Stachniak, T.J., Ghosh, A., and Sternson, S.M. (2014). Chemogenetic synaptic silencing of neural circuits localizes a hypothalamus→midbrain pathway for feeding behavior. Neuron *82*, 797–808.

58. Campbell, E.J., and Marchant, N.J. (2018). The use of chemogenetics in behavioural neuroscience: receptor variants, targeting approaches and caveats. Br. J. Pharmacol. *175*,

994–1003.

59. Cohen, S.R., and Melzack, R. (1985). Morphine injected into the habenula and dorsal posteromedial thalamus produces analgesia in the formalin test. Brain Res. *359*, 131–139.

60. Han, S., Soleiman, M.T., Soden, M.E., Zweifel, L.S., and Palmiter, R.D. (2015). Elucidating an Affective Pain Circuit that Creates a Threat Memory. Cell *162*, 363–374.

61. Chiang, M.C., Nguyen, E.K., Canto-Bustos, M., Papale, A.E., Oswald, A.-M.M., and Ross, S.E. (2020). Divergent Neural Pathways Emanating from the Lateral Parabrachial Nucleus Mediate Distinct Components of the Pain Response. Neuron *106*, 927–939.e5.

62. Fields, H. (2004). State-dependent opioid control of pain. Nat. Rev. Neurosci. *5*, 565–575.

63. François, A., Low, S.A., Sypek, E.I., Christensen, A.J., Sotoudeh, C., Beier, K.T., Ramakrishnan, C., Ritola, K.D., Sharif-Naeini, R., Deisseroth, K., et al. (2017). A Brainstem-Spinal Cord Inhibitory Circuit for Mechanical Pain Modulation by GABA and Enkephalins. Neuron *93*, 822–839.e6.

64. Finn, D. (2017). The impact of stress on pain. Physiology News, 25–27. 10.36866/pn.108.25.

65. Vaccarino, A.L., Marek, P., Sternberg, W., and Liebeskind, J.C. (1992). NMDA receptor antagonist MK-801 blocks non-opioid stress-induced analgesia in the formalin test. Pain *50*, 119–123.

66. Lewis, J.W., Sherman, J.E., and Liebeskind, J.C. (1981). Opioid and non-opioid stress analgesia: assessment of tolerance and cross-tolerance with morphine. J. Neurosci. *1*, 358–363.

67. Callaway, E.M., and Luo, L. (2015). Monosynaptic Circuit Tracing with Glycoprotein-Deleted Rabies Viruses. J. Neurosci. *35*, 8979–8985.

68. Wickersham, I.R., Finke, S., Conzelmann, K.-K., and Callaway, E.M. (2007). Retrograde neuronal tracing with a deletion-mutant rabies virus. Nat. Methods *4*, 47–49.

69. Kim, J., Zhao, T., Petralia, R.S., Yu, Y., Peng, H., Myers, E., and Magee, J.C. (2011). mGRASP enables mapping mammalian synaptic connectivity with light microscopy. Nat. Methods *9*, 96–102.

70. Fields, H.L., Malick, A., and Burstein, R. (1995). Dorsal horn projection targets of ON and OFF cells in the rostral ventromedial medulla. Journal of Neurophysiology *74*, 1742–1759. 10.1152/jn.1995.74.4.1742.

71. Fields, H.L., Heinricher, M.M., and Mason, P. (1991). Neurotransmitters in nociceptive modulatory circuits. Annu. Rev. Neurosci. *14*, 219–245.

72. Nguyen, E., Smith, K.M., Cramer, N., Holland, R.A., Bleimeister, I.H., Flores-Felix, K., Silberberg, H., Keller, A., Le Pichon, C.E., and Ross, S.E. (2022). Medullary kappa-opioid receptor neurons inhibit pain and itch through a descending circuit. Brain *145*, 2586–2601.

73. Kondo, Y., Koizumi, T., Arai, Y., Kakeyama, M., and Yamanouchi, K. (1993). Functional relationships between mesencephalic central gray and septum in regulating lordosis in

female rats: Effect of dual lesions. Brain Research Bulletin *32*, 635–638. 10.1016/0361-9230(93)90166-9.

74. Assareh, N., Sarrami, M., Carrive, P., and McNally, G.P. (2016). The organization of defensive behavior elicited by optogenetic excitation of rat lateral or ventrolateral periaqueductal gray. Behav. Neurosci. *130*, 406–414.

75. Liebman, J.M., Mayer, D.J., and Liebeskind, J.C. (1970). Mesencephalic central gray lesions and fear-motivated behavior in rats. Brain Res. *23*, 353–370.

76. Halpern, M. (1968). Effects of midbrain central gray matter lesions on escape-avoidance behavior in rats. Physiology & Behavior *3*, 171–178. 10.1016/0031-9384(68)90050-4.

77. Samineni, V.K., Grajales-Reyes, J.G., Copits, B.A., O'Brien, D.E., Trigg, S.L., Gomez, A.M., Bruchas, M.R., and Gereau, R.W., 4th (2017). Divergent Modulation of Nociception by Glutamatergic and GABAergic Neuronal Subpopulations in the Periaqueductal Gray. eNeuro *4*. 10.1523/ENEURO.0129-16.2017.

78. Maier, S.F., Drugan, R.C., and Grau, J.W. (1982). Controllability, coping behavior, and stress-induced analgesia in the rat. Pain *12*, 47–56.

79. Terman, G.W., and Liebeskind, J.C. (1986). Relation of stress-induced analgesia to stimulation-produced analgesia. Ann. N. Y. Acad. Sci. *467*, 300–308.

80. Wang, D., Pan, X., Zhou, Y., Wu, Z., Ren, K., Liu, H., Huang, C., Yu, Y., He, T., Zhang, X., et al. (2023). Lateral septum-lateral hypothalamus circuit dysfunction in comorbid pain and anxiety. Mol. Psychiatry. 10.1038/s41380-022-01922-y.

81. Watkins, L.R., and Mayer, D.J. (1986). Multiple Endogenous Opiate and Non-Opiate Analgesia Systems: Evidence of Their Existence and Clinical Implications. Annals of the New York Academy of Sciences *467*, 273–299. 10.1111/j.1749-6632.1986.tb14635.x.

82. Drugan, R.C., Grau, J.W., Maier, S.F., Madden, J., 4th, and Barchas, J.D. (1981). Cross tolerance between morphine and the long-term analgesic reaction to inescapable shock. Pharmacol. Biochem. Behav. *14*, 677–682.

83. Maier, S.F., Davies, S., Grau, J.W., Jackson, R.L., Morrison, D.H., Moye, T., Madden, J., 4th, and Barchas, J.D. (1980). Opiate antagonists and long-term analgesic reaction induced by inescapable shock in rats. J. Comp. Physiol. Psychol. *94*, 1172–1183.

84. Grau, J.W., Hyson, R.L., Maier, S.F., Madden, J., 4th, and Barchas, J.D. (1981). Long-term stress-induced analgesia and activation of the opiate system. Science *213*, 1409–1411.

85. Rubinstein, M., Mogil, J.S., Japón, M., Chan, E.C., Allen, R.G., and Low, M.J. (1996). Absence of opioid stress-induced analgesia in mice lacking beta-endorphin by site-directed mutagenesis. Proc. Natl. Acad. Sci. U. S. A. *93*, 3995–4000.

86. Reynolds, D.V. (1969). Surgery in the rat during electrical analgesia induced by focal brain stimulation. Science *164*, 444–445.

87. Olango, W.M., and Finn, D.P. (2014). Neurobiology of stress-induced hyperalgesia. Curr. Top. Behav. Neurosci. *20*, 251–280.

88. Owens-French, J., Li, S.-B., Francois, M., Leigh Townsend, R., Daniel, M., Soulier, H., Turner, A., de Lecea, L., Münzberg, H., Morrison, C., et al. (2022). Lateral hypothalamic galanin neurons are activated by stress and blunt anxiety-like behavior in mice. Behav. Brain Res. *423*, 113773.

89. Wang, D., Li, A., Dong, K., Li, H., Guo, Y., Zhang, X., Cai, M., Li, H., Zhao, G., and Yang, Q. (2021). Lateral hypothalamus orexinergic inputs to lateral habenula modulate maladaptation after social defeat stress. Neurobiol Stress *14*, 100298.

90. Moga, M.M., Saper, C.B., and Gray, T.S. (1990). Neuropeptide organization of the hypothalamic projection to the parabrachial nucleus in the rat. The Journal of Comparative Neurology *295*, 662–682. 10.1002/cne.902950409.

91. Pelosi, G.G., Tavares, R.F., and Corrêa, F.M.A. (2006). Rostrocaudal somatotopy in the neural connections between the lateral hypothalamus and the dorsal periaqueductal gray of the rat brain. Cell. Mol. Neurobiol. *26*, 635–643.

92. Cassidy, R.M., Lu, Y., Jere, M., Tian, J.-B., Xu, Y., Mangieri, L.R., Felix-Okoroji, B., Selever, J., Xu, Y., Arenkiel, B.R., et al. (2019). A lateral hypothalamus to basal forebrain neurocircuit promotes feeding by suppressing responses to anxiogenic environmental cues. Sci Adv *5*, eaav1640.

93. Mathis, A., Mamidanna, P., Cury, K.M., Abe, T., Murthy, V.N., Mathis, M.W., and Bethge, M. (2018). DeepLabCut: markerless pose estimation of user-defined body parts with deep learning. Nat. Neurosci. *21*, 1281–1289.

94. Susaki, E.A., Shimizu, C., Kuno, A., Tainaka, K., Li, X., Nishi, K., Morishima, K., Ono, H., Ode, K.L., Saeki, Y., et al. (2020). Versatile whole-organ/body staining and imaging based on electrolyte-gel properties of biological tissues. Nat. Commun. *11*, 1982.

Figure 1

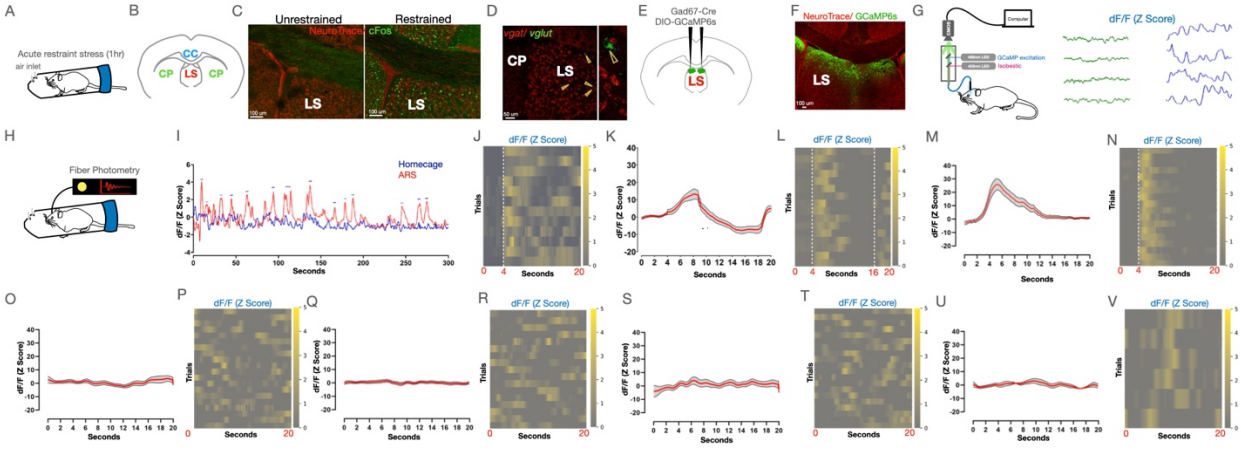

Figure 2

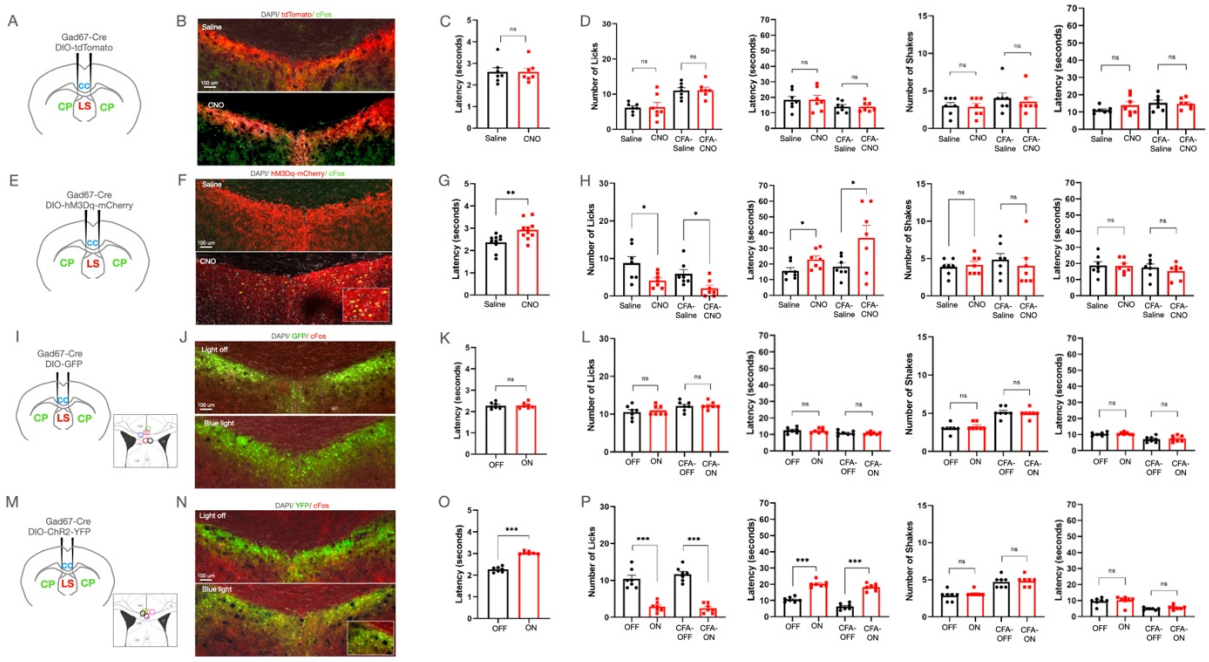

Supplementary Figure 1

LS is sufficient for acute restraint stress induced analgesia

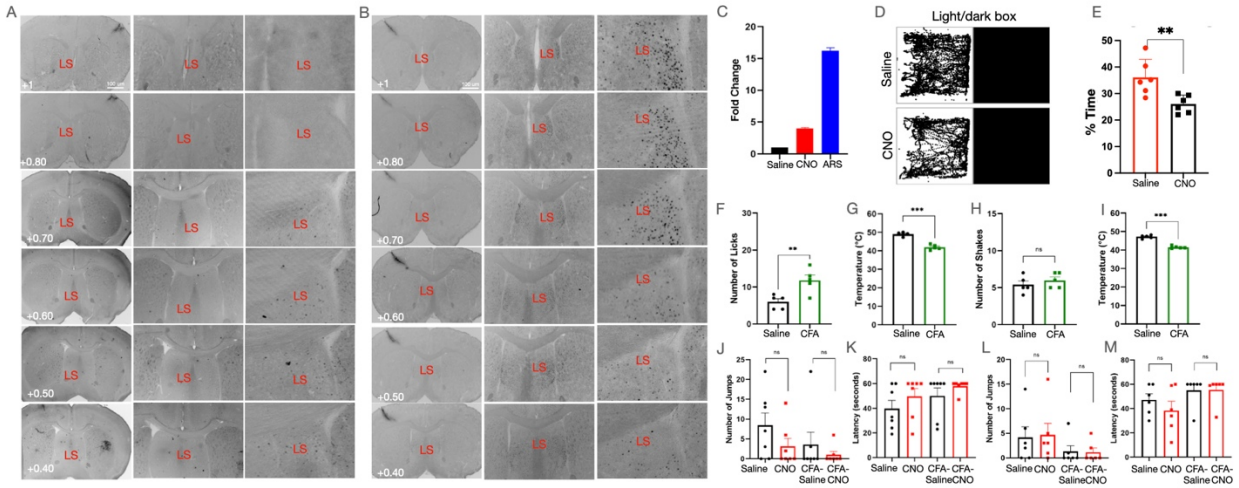

Figure 3

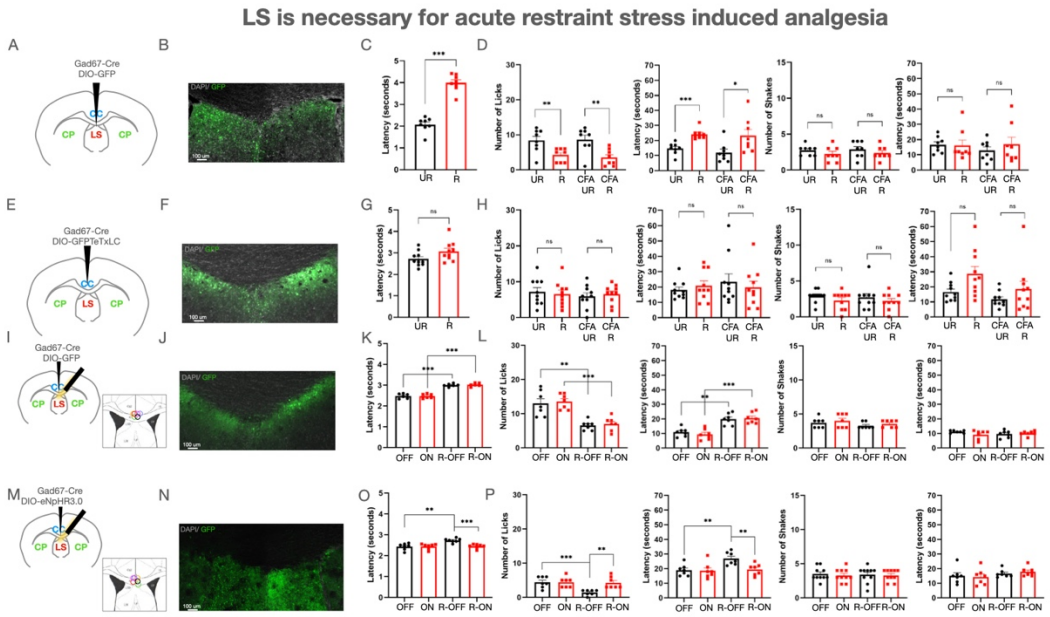

Supplementary Figure 2

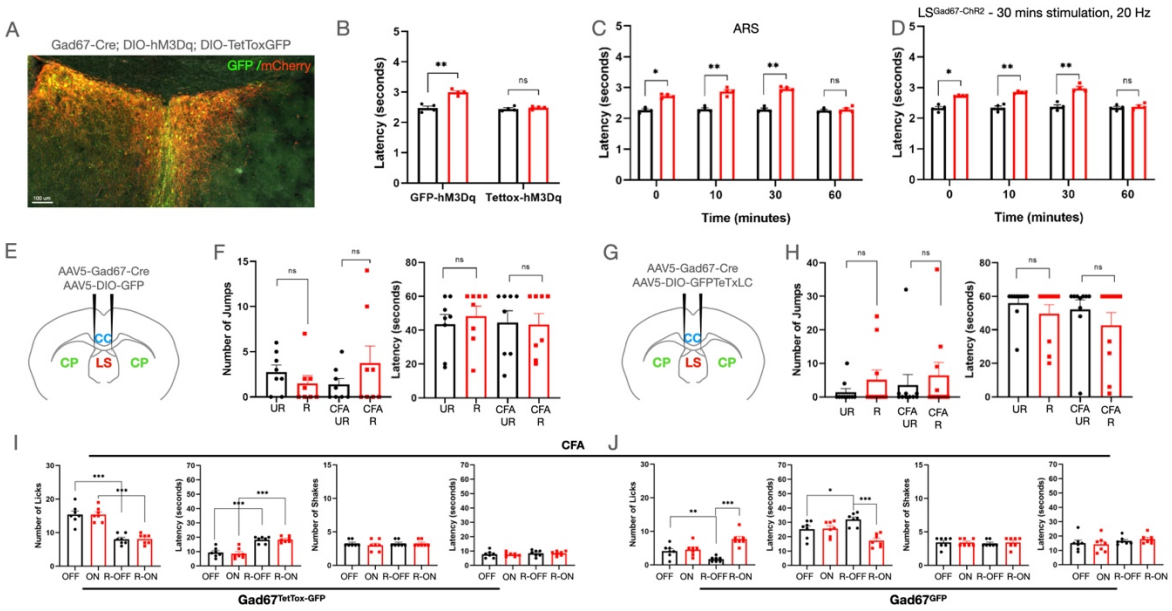

Figure 4

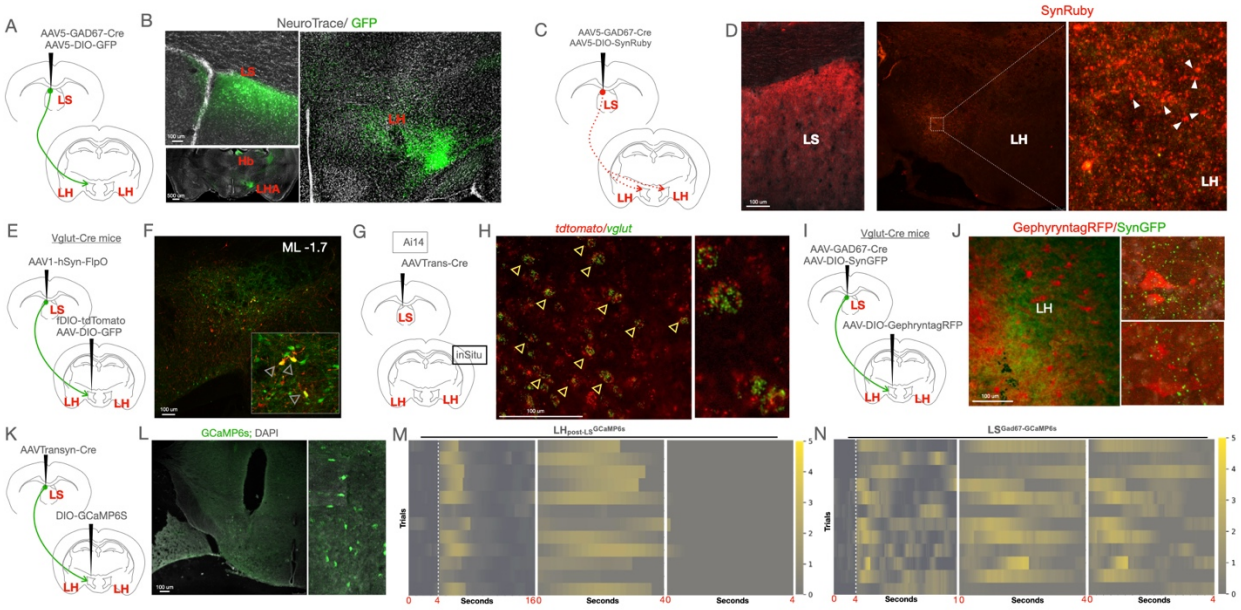

Supplementary Figure 3

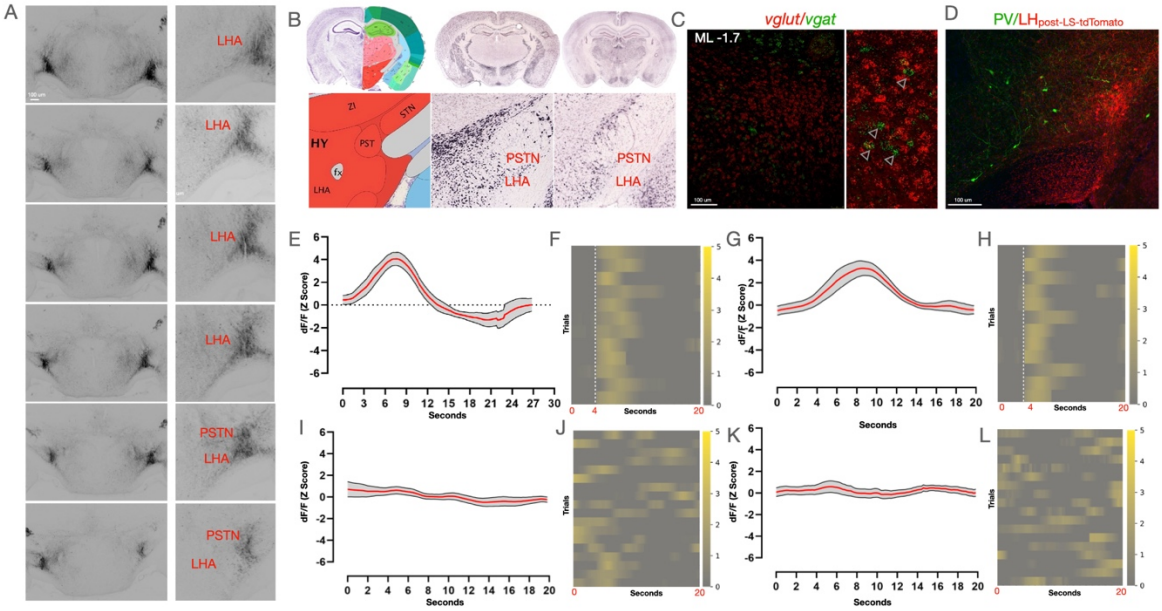

Figure 5

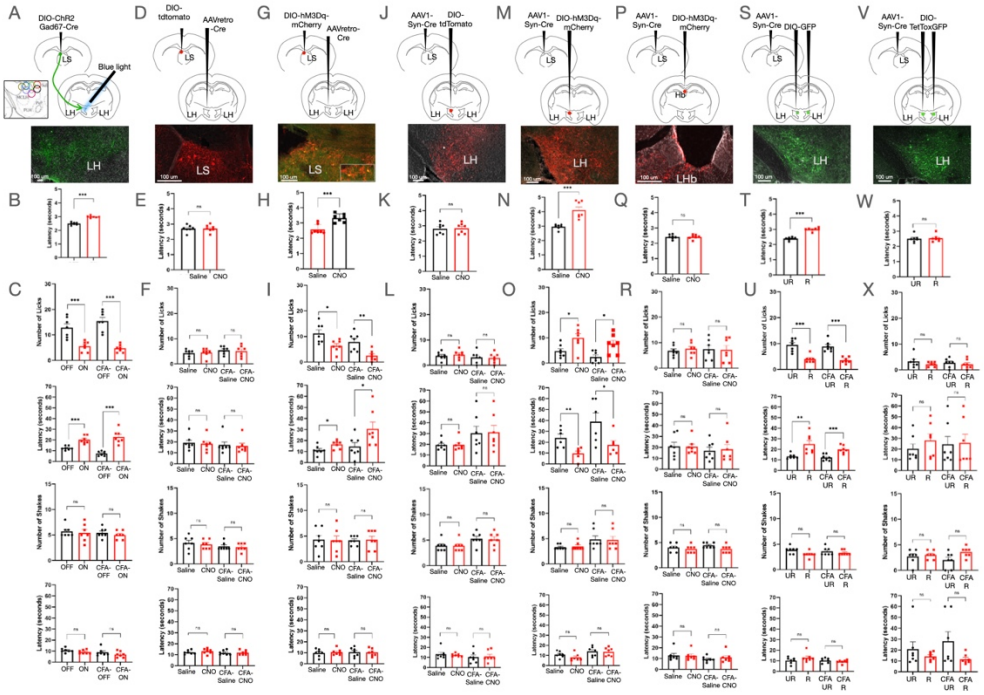

Supplementary Figure 4

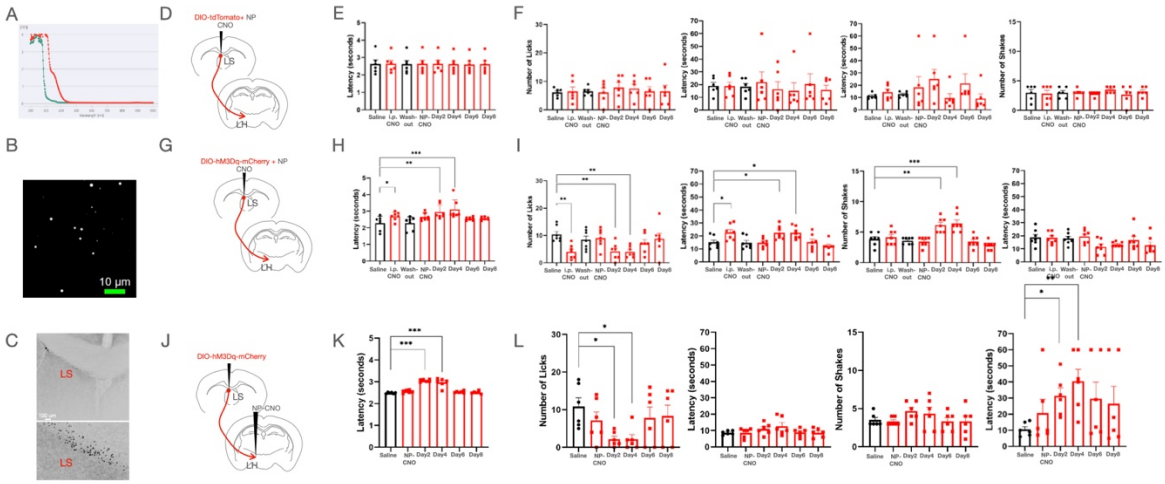

Figure 6

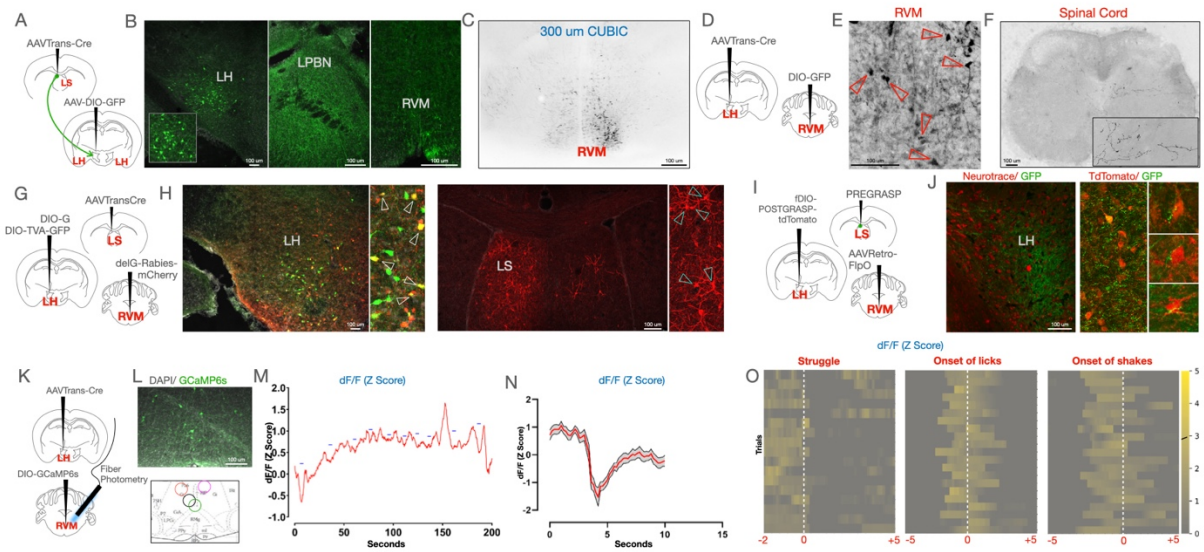

Supplementary Figure 5

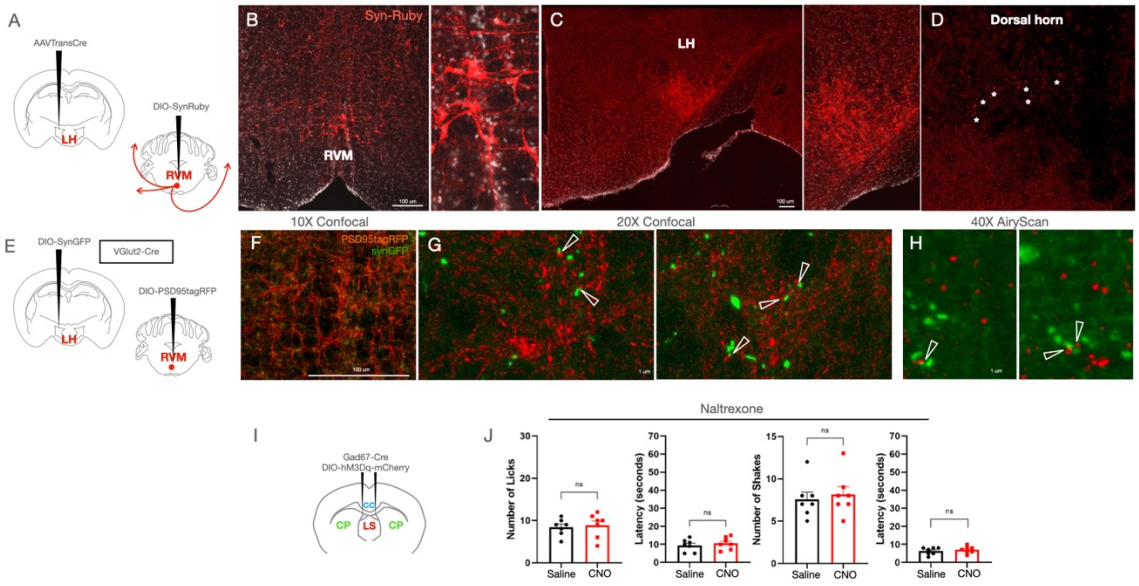

Figure 7

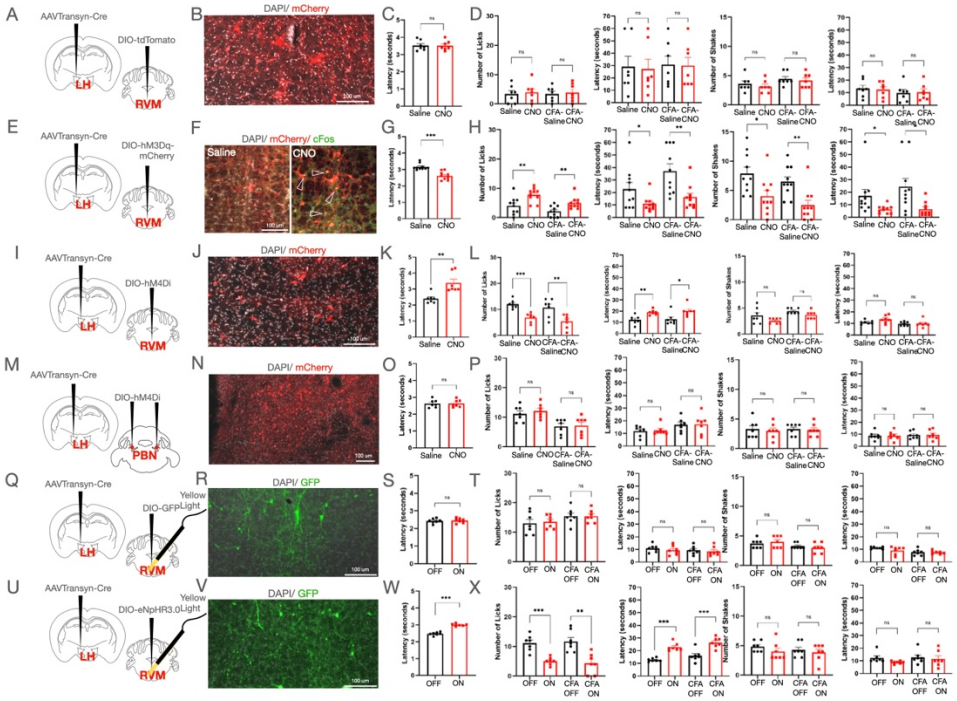

Figure 8

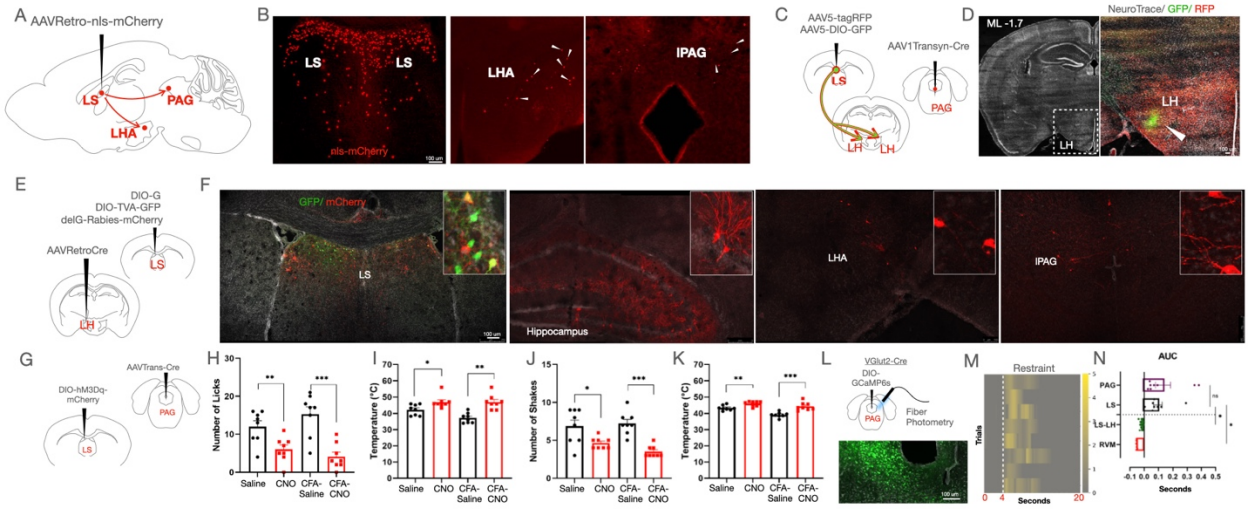

Supplementary Figure 6